Pergamon

Progress in Oceanography 43 (1999) 55–109

Progress in Oceanography

Circulation, mixing, and production of Antarctic Bottom Water

A.H. Orsi[a,*1], G.C. Johnson[b], J.L. Bullister[b]

[a]*Joint Institute for Study of the Atmosphere and Ocean, University of Washington, Seattle, WA 98125, USA*

[b]*Pacific Marine Environmental Laboratory, NOAA, Seattle, WA 98115-0070, USA*

Abstract

The Antarctic source of bottom water to the abyssal layer of the World Ocean is examined, as well as its large-scale flow pattern and ultimate entrainment rate into the deep water above. We make use of the available high-quality station data in the Southern Ocean to construct bottom maps of neutral density and mean property maps, including Chlorofluorocarbon (CFC), for the abyssal layer underneath a selected neutral density surface. The maximum density at the sill depth of Drake Passage is used to distinguish between the voluminous deep water mass that is a continuous component of the Antarctic Circumpolar Current from the relatively denser bottom water originated along the Antarctic continental margins. Based on water density, Antarctic Bottom Water (AABW) is defined here generically to include all volumes of non-circumpolar water of Antarctic origin. Over the shelf regime multiple localized sources of specific AABW types contribute to the abyssal layer of the adjacent Antarctic basins. Characteristics of these dense bottom waters reflect closely those observed on the parent Shelf Water mass. Spreading paths of newly-formed deep and bottom waters over the slope regime, and their subsequent oceanic circulation patterns are analyzed on the basis of global property maps for the AABW layer. Interior mixing and interbasin exchanges of AABW are deduced from mean characteristic curves following the southern streamline of the Antarctic Circumpolar Current. Outflow and mixing of AABW from the Weddell Sea to the Argentine Basin is depicted using density and CFC distributions of two zonal hydrographic lines. Recirculation and mixing of deep and bottom waters within the Weddell Gyre are also detailed using a meridional section along the Greenwich Meridian. The strength of all localized sources of AABW combined is estimated by two independent approaches. An estimate of the total production rate of AABW is calculated based on the oceanic CFC budget for the AABW layer offshore of the 2500-m isobath. The sum of all downslope inputs of well-ventilated bottom

* Corresponding author.

[1] Department of Oceanography, Texas A&M University, College Station, TX 77843-3146, USA. E-mail: aorsi@tamu.edu

PII: S0079-6611(99)00004-X

water types underneath the top isopycnal must account for the measured CFC content in the bottom layer. The resulting total AABW production rate is about 8 Sv, which is a conservative figure that neglects the loss of CFC-bearing waters across the top isopycnal in recent years, whereas about 9.5 Sv is calculated assuming a well-mixed bottom layer. Making use of their transient nature, CFC distributions at the top of the AABW layer indicate that more direct and rapid entrainment of CFC-rich bottom waters below occurs over localized areas with relatively strong upwelling rates and enhanced vertical mixing. A second, more ad-hoc but independent oceanic mass budget of the bottom layer is also constructed. A typical basin-wide rate of deep upwelling of 3×10^{-7} m s^{-1} requires 10 Sv (1 Sv $= 10^6$ m^3 s^{-1}) of newly-formed AABW to sink down the slope around Antarctica. We have also formulated a spatial distribution of deep upwelling on the isopycnal at the top of the AABW. It is expressed as a combination of wind, topographic, and turbulent components, which in turn are functions of the isopycnal depth, bottom depth, and bottom layer thickness. This non-uniform upwelling field yields about 12 Sv of AABW exported across the top isopycnal. Fortuitously, the overall average of upward speed at the top isopycnal (3.7×10^{-7} m s^{-1}) compares well with previous estimates of deep upwelling in the northern basins. A series of likely sites for strong vertical entrainment of AABW are clearly identified in the modeled distribution of deep upwelling, consonant with the observed CFC distributions on the top isopycnal. Altogether, regions with relatively high upwelling rates ($> 5 \times 10^{-7}$ m s^{-1}) occupy only a quarter of the total areal extent of the top isopycnal, but they account for as much as 45% of the total vertical transport.

Contents

1. Introduction

At a few locations around the Antarctic continental margins and in the northern North Atlantic, upper layer waters lose sufficient buoyancy from air–sea and sea–ice exchanges to sink to abyssal depths. These bottom waters move away from the sinking regions in narrow western boundary currents in all three oceans (Warren, 1981a). Thought to be supplied by abyssal boundary current systems are weaker poleward recirculations within the interior of the basins, where deep waters slowly upwell into the upper levels to balance the downward heat flux from the low latitude atmosphere. Relatively warm waters in the upper layer are advected poleward and begin the cycle anew (Stommel, 1958; Stommel & Arons, 1960a, b; Schmitz, 1995). Such a pattern of buoyancy forcing and meridional flow is known as the Global Thermohaline Circulation, a key component in the regulation of the Earth's climate.

The major role played by the sinking and spreading of southern bottom water was clear in the early observations. Wüst (1933) noticed that most of the abyssal layer in the Atlantic Ocean is filled from the south, by a water mass with origin in the high southern latitudes and with characteristics significantly different (lower temperature and salinity) from the northern bottom water. The two bottom waters first meet at low latitudes, where the less dense northern water is displaced off the bottom by the relatively colder southern bottom water flowing to the north. The northern water mass continues southward at mid depths, where it is called the North Atlantic Deep Water (NADW), eventually to enter the Antarctic Circumpolar Current (ACC) in the southwestern Argentine Basin. From there NADW is carried eastward around Antarctica, mixing along its path with less dense deep waters imported from the Indian and Pacific oceans and also with the colder southern bottom water beneath it. Sverdrup (1940) differentiated this uniform, voluminous mixing product, which is recirculating within the ACC, from its parent water masses calling it the Circumpolar Deep Water (CDW). (Uniformity non withstanding, the NADW influence to the CDW is recognizable everywhere in the ACC by its characteristic deep salinity maximum; Reid & Lynn, 1971.) In turn, the subpolar circulations located between Antarctica and the ACC gain CDW from that current and carry it toward the continental margins. At a few sites these diluted derivatives of North Atlantic Deep Water mix with near-freezing Shelf Water to form the coldest southern bottom water (Reid, 1979).

Bottom waters with a southern origin that are colder than the northern source bottom water, say with temperatures below 2°C, have been referred to generically as 'Antarctic Bottom Water' for quite a long time (Deacon, 1933; Speer & Zenk, 1993). However, as Mantyla and Reid (1983) point out, the bulk of bottom water filling the basins north of the Southern Ocean is not drawn directly from the Antarctic margins. Indeed most of the volume carried equatorward by all of the abyssal Western Boundary Currents in the Southern Hemisphere is exported from deep levels of the ACC, water lying above denser southern bottom water and below the salinity maximum. The last represents a vast source distributed on a circumpolar band located, in most places, far from the Antarctica margins. Thus, at least in the Atlantic, there are two distinct components in the 'southern bottom water': the Circumpolar

Deep Water exported from the ACC, and the relatively denser deep waters exported from the subpolar circulations located in the Antarctic basins to the south of the ACC (Mantyla & Reid, 1983; Schmitz, 1995). Gordon (1971, 1972) reserved the term Antarctic Bottom Water for the latter component, to only include deep waters in the Southern Ocean with potential temperatures less than 0°C. In the Argentine Basin, Reid, Nowlin and Patzert (1977) further distinguished between deep waters entering from the Southeast Pacific Ocean and those from the Weddell Sea by means of their density.

This is a global study aimed at the characterization of Antarctic Bottom Water, describing its general circulation in the Southern Ocean, and assessing its replenishment rate over the Antarctic continental margins. It is based on classical hydrographic data, derived primarily from the National Oceanic Data Center (NODC, 1994). Additional hydrographic data, and all of the Chlorofluorocarbon (CFC) data, were obtained directly from the originators. Addition of data from a series of cruises of the World Ocean Circulation Experiment (WOCE) listed in the Acknowledgments were specially useful. CFC measurements in the Indian and Pacific correspond to that Experiment (1990–1996), whereas those in the Atlantic are mostly pre-WOCE (1984–1989) data. Transient tracer data were individually checked for errors, whereas bottle and low-resolution CTD data were more objectively screened for anomalous profiles based on their temperature–salinity relationship.

The first objective of this work is to present a robust, global definition of Antarctic Bottom Water to differentiate unambiguously dense water produced around Antarctica from Circumpolar Deep Water of the Antarctic Circumpolar Current. Similarly, the densest water of the ACC is distinguished from the northern bottom water. Those tasks are addressed in Section 2, based on the observed densities at the bottom of the World Ocean using a new practical method to approximate isentropic surfaces in the ocean (Jackett & MacDougall, 1997). We also present evidence of the intense mixing between deep and bottom waters taking place over the sill of Drake Passage.

With Antarctic Bottom Water clearly defined, we proceed to describe its regional characteristics and circulation in all three sectors of the Southern Ocean. This work is accomplished in Section 3, by inspection of lateral property distributions on the bottom layer occupied by the Antarctic Bottom Water. In constructing these maps we have made use of all available high quality hydrographic data from south of 30°S (Fig. 1(a)). Changes in the mean temperature–salinity relationship of deep and bottom waters circulating through the southern Indian sector of the ACC are examined to describe exchanges of Antarctic Bottom Water produced in different Antarctic Basins.

In Section 4, Chlorofluorocarbon distributions on selected hydrographic lines are used to describe the ventilation of deep and bottom waters in the South Atlantic by Antarctic Bottom Water exported from the Weddell Sea. One section is used to trace the northward outflow of Weddell Sea waters along the southern Scotia Sea and South Sandwich Trench system, and another to depict its circulation in the southern Argentine Basin. The eastward export of Weddell Sea waters to the Enderby Basin and the westward inflow of new Antarctic Bottom Water originating in the Amery Basin, are investigated along the Greenwich Meridian.

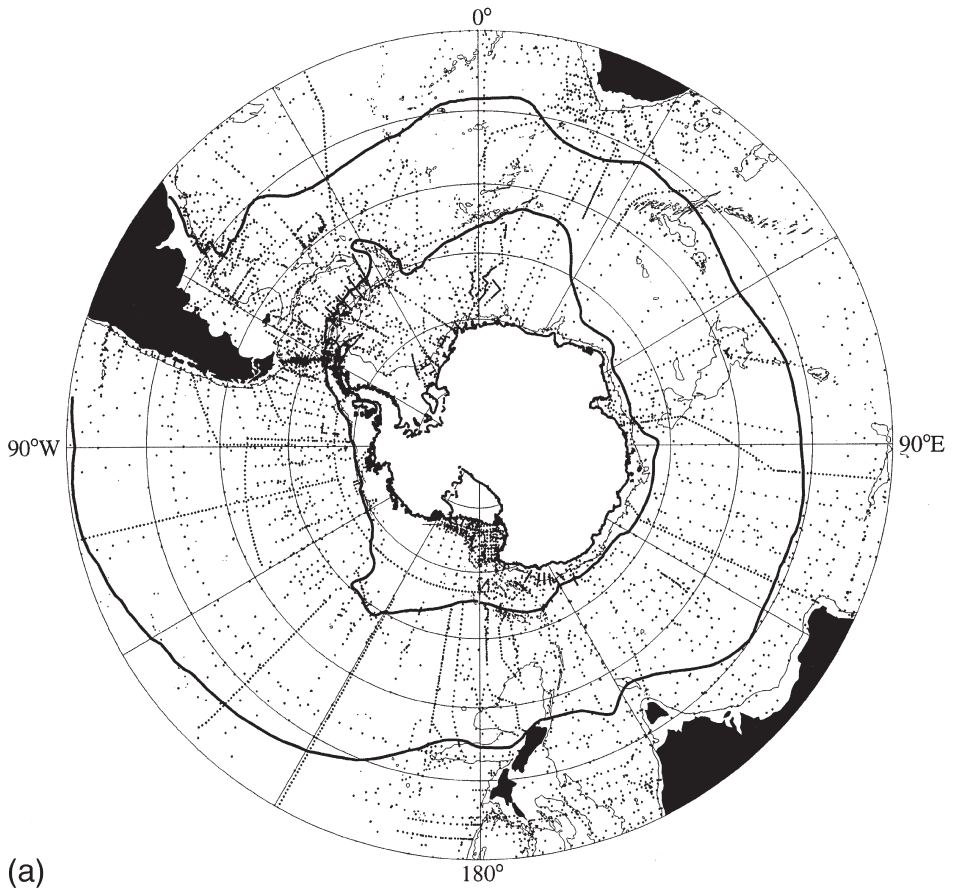

Fig. 1. (a) Map of the Southern Ocean with the hydrographic data used here indicated by the dots. The meridional boundaries of the Antarctic Circumpolar Current are shown as heavy solid lines, as in Orsi, Whitworth and Nowlin (1995); the thin line is the 2-km isobath from GEBCO (IOC, IHO & BODC, 1994).

The final objective of this study, covered in Section 5, is to provide an estimate for the strength of the southern sources of bottom water in the global meridional circulation. One independent estimate of the global production rate of Antarctic Bottom Water is obtained from the CFC inventory for that layer. Previous estimates of the total production rate of Antarctic Bottom Water are compared with those required to balance the volume flux for the oceanic bottom layer from an ad-hoc mixing model. We have organized the presentation so that quantitative results (Section 5) follow the qualitative descriptions (Sections 2–4) of Antarctic Bottom Water.

2. World ocean bottom waters

Paths followed by the densest waters involved in the Global Thermohaline Circulation are clearly identified on property maps near the bottom of the World Ocean

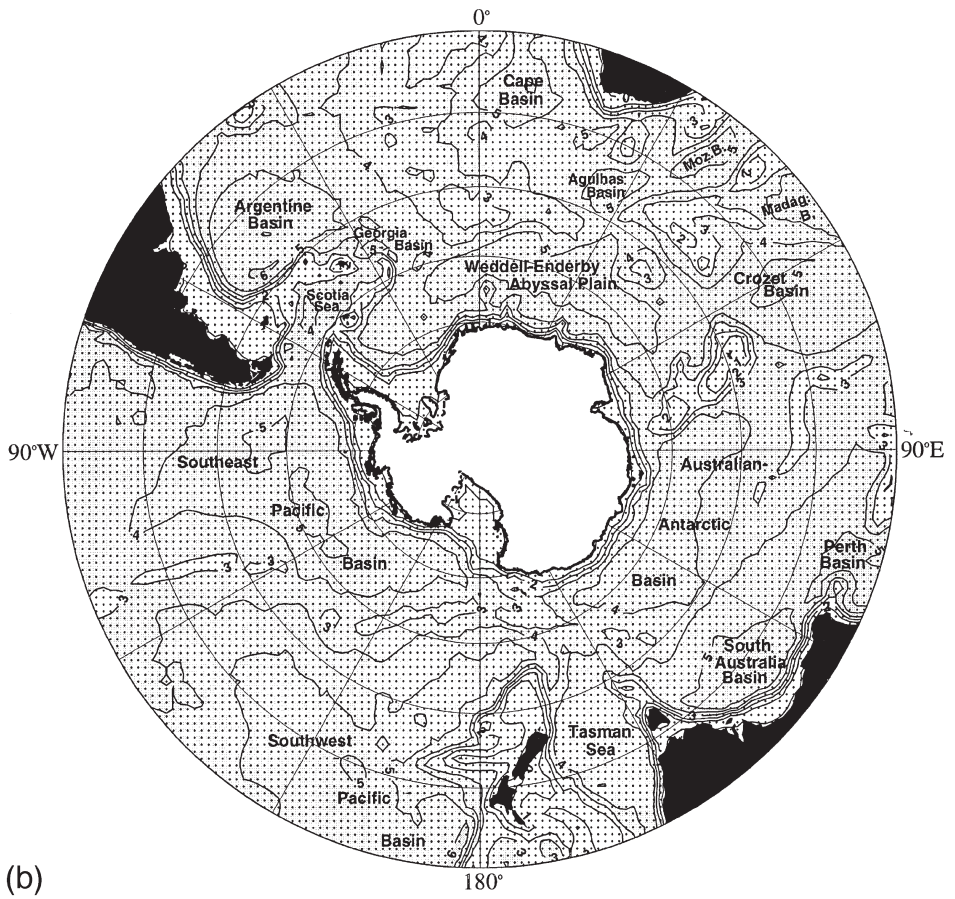

Fig. 1. (b) Stereographic grid adopted for the Southern Ocean, to which property fields were objectively mapped. Isobaths shown at 1-km intervals correspond to the bathymetry interpolated to grid points from 1°-averaged ETOPO5 data. Selected place names are given.

(Wüst, 1935; Lynn & Reid, 1968; Mantyla & Reid, 1983, 1995). The bottom distribution shown in Fig. 2 is of neutral density (γ^n), which is particularly useful while tracing water masses that undergo extreme pressure changes. In contrast to the isopycnal approach based on matching various potential density surfaces with a discrete set of reference pressures, Jackett and MacDougall (1997) computed a neutral density variable that is locally referenced: a well-defined function that incorporates all nonlinear terms in the equation of state for seawater, including the one arising from the pressure dependency of the thermal expansion coefficient. As a reference, Table 1 lists a few neutral density surfaces with their corresponding combinations of the more familiar potential density isopycnals; equivalences are also given in the text.

Bottom maps of density are useful to determine the origin of relatively dense water masses that sink and spread away from their shallower source regions. Two

Table 1
Approximate equivalencies of neutral (γ^n) and potential (σ) density anomalies ranges (in kg m^{-3}), where the σ subscript implies reference pressure in 10^3 dbars

γ^n	σ_0	σ_2	σ_4
28.05	27.77–27.78		
28.10	27.79–27.81	37.05–37.07	
28.15	27.82	37.08–37.10	
28.18	27.83	37.11	
28.20	27.83–27.84	37.12–37.13	
28.25		37.15	46.03–46.05
28.27		37.16	46.04–46.06
28.30		37.17–37.18	46.06–46.10
28.35		37.19–37.21	46.08–46.14
28.40		37.20–37.23	46.12–46.18

distinct sources of bottom waters to the abyssal layer of the World Ocean are evident (Fig. 2) where $\gamma^n > 28.18$ kg m^{-3} ($\sigma_2 \gtrsim 37.11$ kg m^{-3}): a single northern hemisphere source concentrated between Greenland and Iceland, and a southern source that spans nearly all longitudes at 60°S. Both sources supply relatively cold waters to the abyssal boundary currents found at lower latitudes in the North Atlantic and Southern Hemisphere, respectively (Warren, 1981a).

The densest bottom water with a northern origin (Fig. 2; red dots) is directly traced to the Denmark Strait Overflow. This contribution is indicated by the sinking of water with $\gamma^n > 28.18$ kg m^{-3} across the slope (3000-m isobath) toward greater depths south of Greenland; its equatorward extent is near 50°N, perhaps where it meets the North Atlantic Current. In a dramatic contrast, bottom water with a distinct southern origin approaches the Equator with $\gamma^n = 28.18$ kg m^{-3} in all three Oceans: it is carried northward by all the Western Boundary Currents in the Southern Hemisphere. The predominance of southern bottom water in the Atlantic Ocean had already been recognized by Wüst (1933, 1935); and was later described globally in full detail by Mantyla and Reid (1983) using modern data.

Southern bottom water with $28.18 < \gamma^n < 28.27$ kg m^{-3} ($37.11 \lesssim \sigma_2 \lesssim 37.16$ kg m^{-3}) (Fig. 2; red dots) is not exported directly from the abyssal levels of the Antarctic basins, where all bottom waters are actually much denser. Instead it is exported from deep levels at the northern edges of the ACC: most of the volume transported to the north at the western boundary currents is drawn from the lower portion of the Circumpolar Deep Water (Mantyla & Reid, 1983).

Fig. 2. Near-bottom distribution of neutral density (γ^n). Stations shown (dots) have their deepest sample within 200 m of the ocean floor, and are located at water depths greater than 3000 m; exceptions were made for shallower stations located near the source regions, along the Antarctic continental margins and the northern North Atlantic. Only three density classes are indicated by the colored dots: $\gamma^n > 28.27$ kg m^{-3} (blue), $28.18 < \gamma^n < 28.27$ kg m^{-3} (red), and $\gamma^n < 28.18$ kg m^{-3} (black). The 3-km GEBCO isobath is shown as a thin grey line; the global (inset) map is in Gall-Peters equal-area (Mercator) projection. The inset shows the Drake Passage area with the circled red dot indicating sta. 116 from WOCE cruise A21 of 1990 (Roether et al., 1993), and the dark 4500-m isobath enclosing the South Shetland Trench.

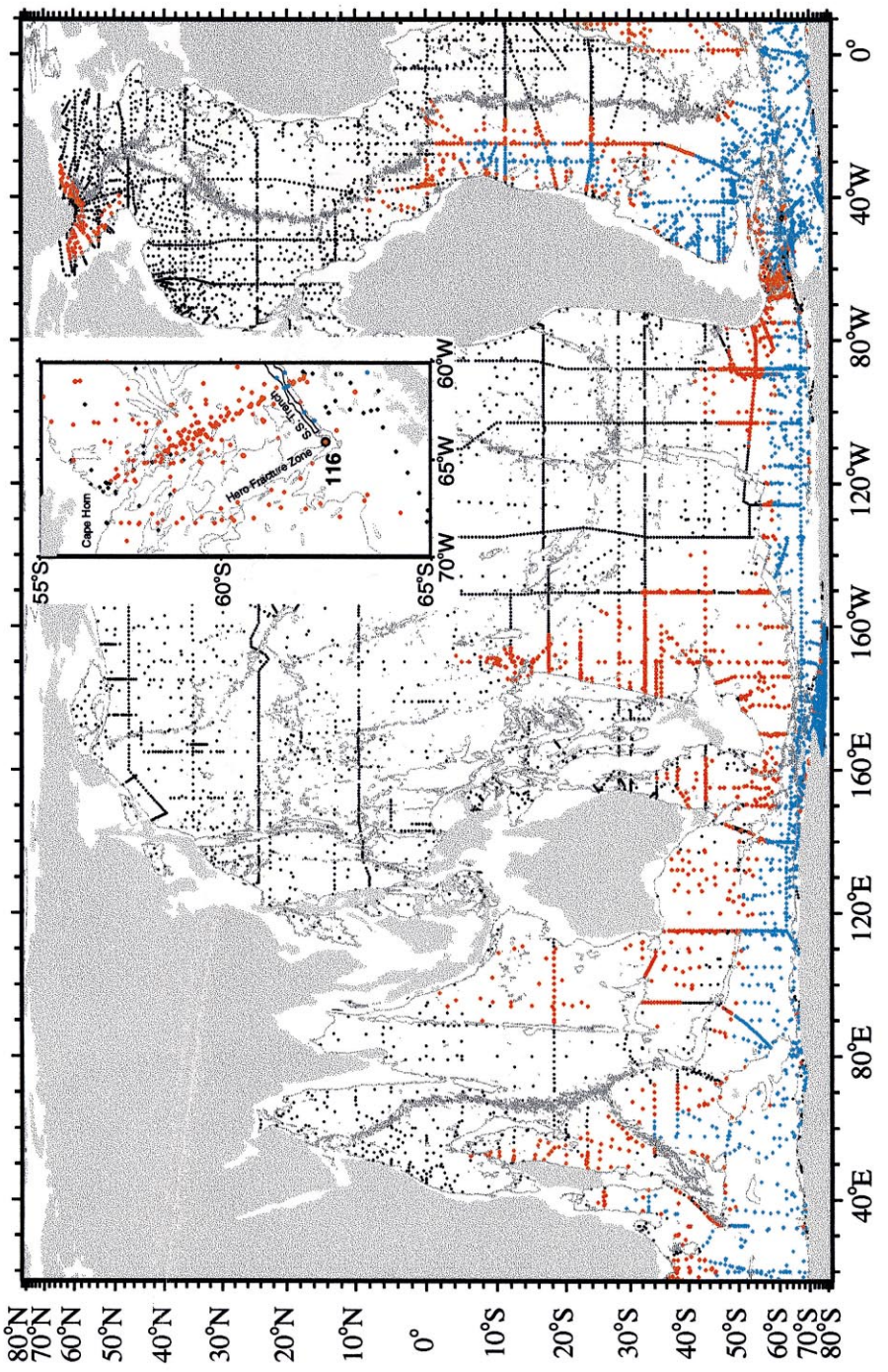
80°N
70°N
60°N
50°N
40°N
30°N
20°N
10°N
0°
10°S
20°S
30°S
40°S
50°S
60°S
70°S
80°S
40°E
80°E
120°E
160°E
160°W
120°W
80°W
40°W
0°
55°S
60°S
65°S
70°W
65°W
60°W
Cape Horn
Hero Fracture Zone
SSS Trench
116

A heavier variety of southern bottom water, with $\gamma^n > 28.27$ kg m^{-3} ($\sigma_2 \gtrsim 37.16$ kg m^{-3}) (Fig. 2; blue dots) is also carried along the branches extending northward into the Argentine, Brazil, Mozambique, and Crozet basins. This relatively dense water is supplied by deep outflows from the Weddell Gyre (Orsi, Nowlin & Whitworth, 1993) that manage to underride the ACC to enter the subtropical regime. Dense Weddell Sea waters overflow into the southern Scotia Sea, in particular through a deep gap in the South Scotia Ridge (Wüst, 1933; Locarnini, Whitworth & Nowlin, 1993). A portion of this overflow continues westward along the deeper portion of the slope (Nowlin & Zenk, 1988), as far east as the Drake Passage (Whitworth, Nowlin & Worley, 1982), where its last remnants fill the bottom of the South Shetland Trench (Sievers & Nowlin, 1984). In contrast to the Weddell–Enderby Basin, bottom water with similar densities ($\gamma^n > 28.27$ kg m^{-3}) are unable to extend beyond (north of) the ridge systems bounding the Australian–Antarctic and Southeast Pacific basins. Thus the bottom branches (Fig. 2; red dots) extending into the West Australian, Tasman, Southwest Pacific and Southeast Pacific basins export only the lighter variety of southern bottom water away from the ACC, i.e. waters with $28.18 < \gamma^n < 28.27$ kg m^{-3} ($37.11 \lesssim \sigma_2 \lesssim 37.16$ kg m^{-3}).

Considerably denser southern bottom waters are confined by the ridge systems and must circulate inside each of the three Antarctic Basins. These heavier local types of bottom water are not distinguished in Fig. 2, but maps in Mantyla and Reid (1995; their Fig. 2) show bottom potential density $\sigma_4 > 46.16$ kg m^{-3} ($\gamma^n \gtrsim 28.36$ kg m^{-3}) as isolated tongues in the Weddell–Enderby Basin as well as in the Australian–Antarctic Basin. Similarly, but based on an older equation of state for seawater, the global distributions given in Carmack (1977; his Fig. 13) and in Mantyla and Reid (1983; their Fig. 2(a)) reveal the confinement of dense bottom waters in the western Southeast Pacific Basin. Despite their all having extreme potential density, there is a remarkable contrast in the characteristics of the bottom waters spreading off different Antarctic shelves (Figs. 10–11 in Carmack, 1977; Fig. 14 in Gordon, 1998; Figs. 5–6 in Rintoul, 1998; Figs. 25–26 in Locarnini, 1994). Bottom water in the southwestern Weddell Sea is the coldest and freshest ($\theta < -1$°C and $S < 34.64$); that in the northwestern Ross Sea is the warmest and saltiest (-0.6°C $< \theta < -0.3$°C and $S > 34.72$), and that off the Adélie Coast (140°–150°E) shows intermediate properties (-0.8°C $< \theta < -0.4$°C and $34.62 < S < 34.68$).

2.1. Antarctic Bottom Water varieties

The two major source waters that participate in the formation of the densest varieties of bottom water at various locations near the Antarctic shelf break are warm remnants of the regional Circumpolar Deep Water ($\theta > 0$°C) that have been imported from the ACC, and extremely cold Shelf Waters ($\theta < -1.7$°C) onshore. Although the complete sequence of processes leading to the formation of bottom water is not fully understood, it seems reasonable to assume that the rate of entrainment of ambient waters through which Shelf Water mixtures sink before reaching the abyssal depths is important.

To describe the multiple contributions of newly-formed bottom water types sinking

away from their shallower shelf sources we have selected a few stations around Antarctica (Fig. 3(a)) to display θ–S relationships (Fig. 3(b)). The trace for the potential density surface with $\sigma_4 = 46.16$ kg m^{-3} ($\gamma^n \approx 28.36$ kg m^{-3}) is included because the volumes of newly-formed bottom water found below this deep isopycnal are not able to outflow the Antarctic basin where they are observed. The saltiest variety, seen at sta. 154 near 172°E, is called Ross Sea Bottom Water and derives ultimately from the saltiest Shelf Waters ($S > 34.8$), which occur over the western Ross Sea (Jacobs, Amos & Bruchhausen, 1970). In contrast, Shelf Waters with considerably lower salinities are found at several locations (Gordon, 1971). Consequently, it is not surprising that the relatively fresh types of bottom water are found widely around Antarctica. Gordon (1974) notes that the western periphery of the Weddell Sea, the Amery and Shackleton Ice Shelf regions, the Adélie Coast, and the eastern Ross Sea are among the locations most likely producing low-salinity types of bottom water. Jacobs, Amos & Bruchhausen (1970) also observed low salinity Ross Sea Bottom Water in the eastern Ross Sea, as depicted at sta. 82 near 175°W. Rintoul and Bullister (1999) found Adélie Land Bottom Water at their sta. 27 near 137°E, with even lower salinity than had previously been reported by Gordon and Tchernia (1972) in the same area. Practically identical bottom water properties are found at sta. 242 near 60°E (Jacobs & Georgi, 1977), and in the Weddell Sea Bottom Water at sta. 29 in the southwestern Weddell Sea (Foster & Carmack, 1976). Gordon, Huber, Hellmer & Ffield (1993) also showed Weddell Sea Bottom Water with very low salinity in the northwestern Weddell Sea, as indicated by the bottom layer with $S < 34.63$ and $\theta < -0.8$°C at their sta. 61 (Ice Station Weddell of 1992). Only this low-salinity variety formed in the Weddell Sea with $\gamma^n > 28.27$ kg m^{-3} can flow into the adjacent northern basins (Fig. 2). Note also the relatively large temperature and salinity range in the temperature maximum of the Circumpolar Deep Water available for bottom water formation at these shelves (Whitworth, Orsi, Kim, Nowlin & Locarnini, 1998).

2.2. Antarctic Bottom Water: definition revisited

The sill of Drake Passage acts as an effective block to any circumpolar exchange of the relatively denser bottom water of southern origin shown in Fig. 2 (blue dots; see inset). No bottom water with $\gamma^n > 28.27$ kg m^{-3} ($\sigma_2 \gtrsim 37.16$ kg m^{-3}) is seen to flow over the top of the Hero Fracture Zone (65°W), either from the Atlantic or from the Pacific sectors of the ACC. Only the slightly less dense Southeast Pacific Deep Water (Sievers & Nowlin, 1984) is able to overpass this sill, and continues within the circumpolar current into the Scotia Sea. In the Argentine Basin Reid et al. (1977) used potential density $\sigma_4 = 46.06$ kg m^{-3}, reduced here by 0.04 kg m^{-3} to correct to the 1980 International Equation of State, to distinguish Circumpolar Deep Water from the denser Weddell Sea Deep Water that outflows the Weddell Gyre via the South Sandwich Trench and Georgia Basin. A deep relative maximum in the vertical gradient of density was consistently found near that isopycnal (Reid et al., 1977 stratum number 7; Schlemmer, 1978 third stratum; Sievers & Nowlin, 1984 stratum K). Furthermore, Schlemmer (1978) claimed that his third stability maximum

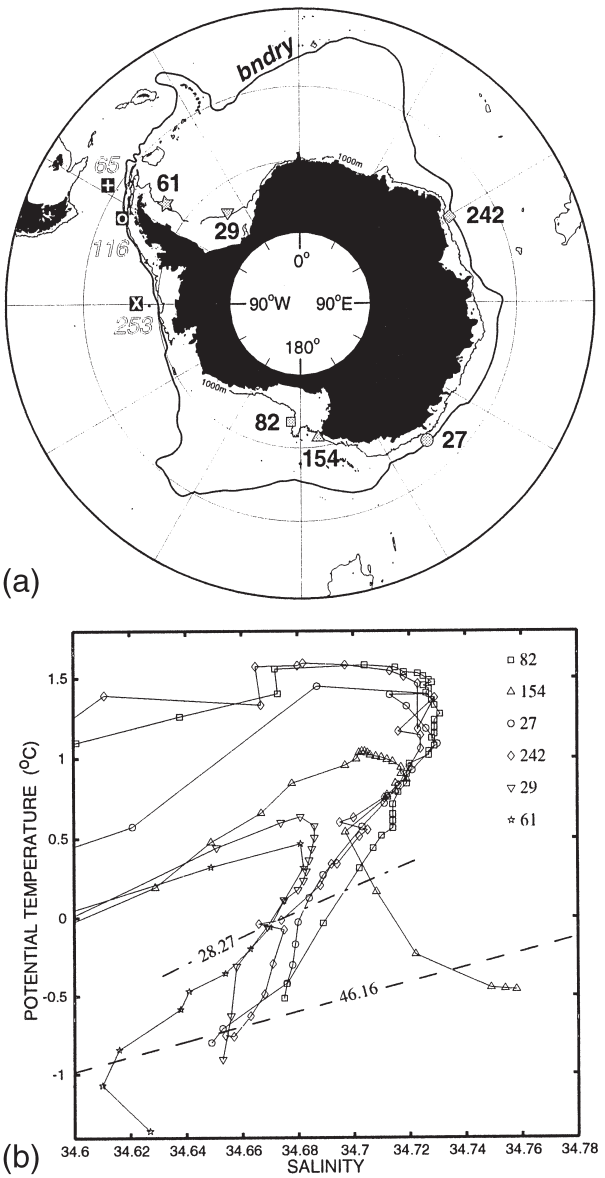

Fig. 3. (a) Top: Locations of selected stations occupied over the deep Antarctic slope domain: sta. **82** from the Northwind cruise 77 of 1977 (Jacobs & Haines, 1982), sta. **154** from Burton Island cruise 78 of 1978 (Jacobs & Haines, 1982), sta. **27** from Aurora Australis WOCE cruise SR3 of 1992 (Rintoul & Bullister, 1999), sta. **242** from Conrad cruise 17 of 1974 (Jacobs & Georgi, 1977), sta. **29** from Glacier of 1973 (Foster & Carmack, 1976), and sta. **61** from Ice Station Weddell of 1992 (Gordon, Huber, Hellmer & Ffield, 1993). Three selected stations located within oceanic domain of the southern ACC are also shown: sta. **116** (○) from Drake Passage (Fig. 2 inset), sta. **65** (+) from the Scotia Sea (Melville cruise FDRAKE of 1975, located at 58.16°W and 58.82°S; Nowlin, Whitworth & Pillsbury, 1977), and sta. **253** (×) from the Bellingshausen Sea (Eltanin cruise 11 of 1964, located at 89.75°W and 67.12°S; Jacobs, 1965). The thick line is the southern boundary of the Antarctic Circumpolar Current, as in Orsi et al. (1995), whereas the thin line is the 1000-m isobath. (b) Bottom: Deep characteristic θ–S diagrams of selected slope stations. The traces of two selected density surfaces, $\gamma^n = 28.27$ kg m^{-3} and $\sigma_4 = 46.16$ kg m^{-3}, are indicated.

could be found in all of the Antarctic basins, thus possibly separating circumpolar water from relatively denser varieties of regional bottom waters.

We reserve the generic term of Antarctic Bottom Water (AABW) to embody the total volume of southern bottom waters that are denser than the Circumpolar Deep Water of the Antarctic Circumpolar Current, i.e. with $\gamma^n \geq 28.27$ kg m^{-3} ($\sigma_2 \gtrsim 37.16$ kg m^{-3}, $\sigma_4 \gtrsim 46.04$–46.06 kg m^{-3}). As in Section 2.1, the use of descriptive regional names is often preferred for the varieties of AABW formed at specific locations around Antarctica. The spatial distribution of AABW is not circumpolar (Fig. 2). Thus we use the surface with $\gamma^n = 28.27$ kg m^{-3} to separate AABW from the overlying Circumpolar Deep Water that flows eastward within the ACC. Fig. 4 shows the deep θ–S scatter for all Drake Passage stations shown in the inset of Fig. 2; the dash-doted lines are polynomial fits to all θ–S pairs in the Southern Ocean interpolated to the $\gamma^n = 28.27$ kg m^{-3} and $\gamma^n = 28.18$ kg m^{-3} surfaces, and the dashed line is the trace of the potential density surface with $\sigma_4 = 46.06$ kg m^{-3}. Only the few stations in the deep South Shetland Trench have bottom densities greater than 28.27 kg m^{-3}—a rather thin bottom layer filled with the westernmost remnant of AABW from the Atlantic sector, namely Weddell Sea Deep Water. The eastern origin of the bottom water in the Trench is clearly demonstrated by the dense, cold and fresh characteristic of the outflowing Weddell Sea Deep Water ($\gamma^n >$

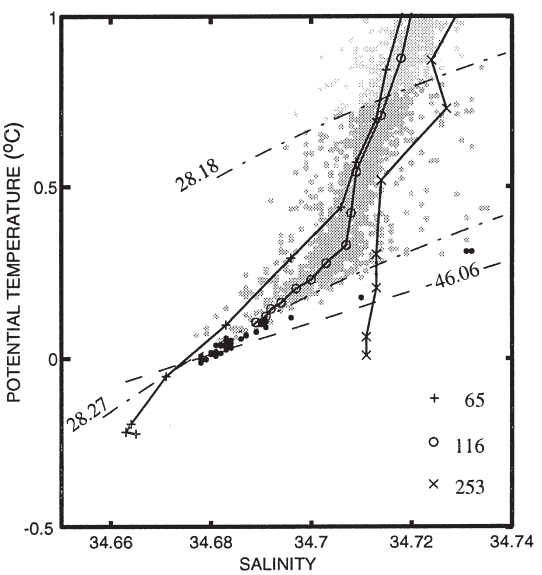

Fig. 4. Deep characteristic θ–S scatter plot for all Drake Passage stations shown in Fig. 2 inset, located between 70°–60°W and 65°–55°S. The traces of two selected neutral density surfaces are shown: $\gamma^n = 28.27$ kg m^{-3}, defining the top of Antarctic Bottom Water, and $\gamma^n = 28.18$ kg m^{-3}, defining the top of ACC bottom water; θ–S pairs are shaded according to their neutral density values for the three ranges defined by these isopycnals. The solid curves joining symbols indicate the traces for the three selected ACC stations shown in Fig. 3(a). The trace of $\sigma_4 = 46.06$ kg m^{-3} potential density surface is also included for reference.

28.27 kg m^{-3}) at sta. 65, located in the southwestern Scotia Sea just to the east of the Shackleton Fracture Zone (see Fig. 3(a) for station locations).

2.3. Lateral mixing

Intense lateral mixing is implied at Drake Passage within the bottom portion of Circumpolar Deep Water. In contrast to the rather homogenous water found below the sill depth in the South Shetland Trench stations, Drake Passage stations (Fig. 4) reveal a saltier and less uniform bottom layer of Lower Circumpolar Deep Water entering from the Southeast Pacific Basin. Sta. 253 (see Fig. 3(a) for locations) provides an example of the typical characteristics seen in the Lower Circumpolar Deep Water and Ross Sea Bottom Water ($\gamma^n > 28.27$ kg m^{-3}) of the Bellingshausen Basin. A downward increase in the θ–S scatter appears to start at inflection points seen on the deep curves, say at potential temperatures between 0.3°C and 0.5°C. Furthermore, a freshening of Lower Circumpolar Deep Water must occur rapidly during its relatively short transit through Drake Passage; a process that is clear in the downstream (see Fig. 3(a)) progression of the three deep characteristic curves shown in Fig. 4: station 116, which is located over the Hero Fracture Zone just west of the South Shetland Trench, reflects the immediate transition from the saline Bellingshausen curve (sta. 253) to the low-salinity Scotia curve (sta. 65) at potential temperatures below 0.3°C.

Water masses constantly mix with the adjacent waters as they move, so any regional definition of AABW based on a fixed temperature value will inevitably fail if applied over larger areas of the ocean. For instance, there is Lower Circumpolar Deep Water as cold as 0°C in the Scotia Sea that could actually flow uninterrupted around Antarctica; whereas there is also AABW as warm as 0.2°C in the Bellingshausen Basin that can not continue eastward over the sill of Drake Passage, unless modified. Likewise a parcel of water at the top of the AABW layer following the path of the ACC will constantly warm up by mixing with the waters above, and if its net heat gain is large enough to lower its density, then this AABW could eventually be entrained into the bottom layer of the Circumpolar Deep Water—a replenishment mechanism for the latter water mass. Hence we adopt the $\gamma^n = 28.27$ kg m^{-3} isopycnal ($\sigma_2 \approx 37.16$ kg m^{-3}, $\sigma_4 \approx 46.04$–46.06 kg m^{-3}) as an upper boundary for AABW.

Mean θ–S curves (Fig. 5) for stations within four distinct sectors of the ACC reveal the progressive eastward warming and salinification along isopycnals within the Lower Circumpolar Deep Water with $28.18 < \gamma^n < 28.27$ kg m^{-3}. These sectors are delimited by the major bathymetric constraints (see Fig. 1(a)) for continuous eastward flow of deep and bottom waters around Antarctica. The dot-dashed curve of the Atlantic sector (60°W–80°E) gradually changes, through the Indian sector (80°–160°E) represented by the solid curve, toward the dashed curve of the Pacific sector (160°E–70°W). In contrast, the dotted curve of the Drake Passage (70°–60°W, 65°–55°S) confirms the remarkably rapid freshening resulting from locally intensified mixing on isopycnals lying very close to $\gamma^n = 28.27$ kg m^{-3} ($\sigma_2 \approx 37.16$ kg m^{-3}). It takes a much longer transit through the entire Indian sector of the ACC for the

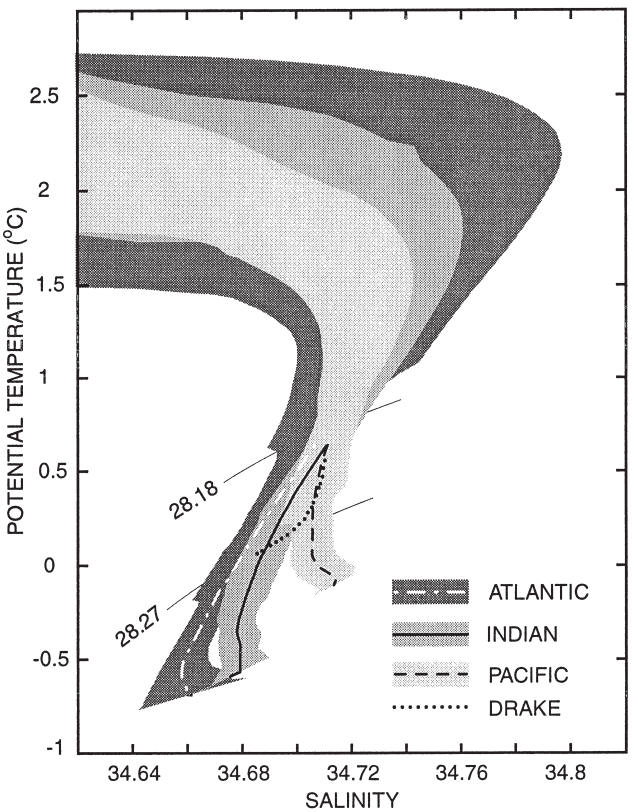

Fig. 5. Mean characteristic θ–S diagrams for deep waters at stations located within the ACC, as in Fig. 1(a), here divided into three Ocean sectors and Drake Passage as follows: Atlantic (60°W–80°E), Indian (80°–160°E), Pacific (160°E–70°W), and Drake Passage (70°–60°W, 65°–55°S). The gray-shaded envelope for each Ocean sector is one standard deviation around the mean curve; all statistics are computed at a selected set of neutral density surfaces. The traces of $\gamma^n = 28.27$ kg m^{-3} and $\gamma^n = 28.18$ kg m^{-3} are included as thin lines in the background.

densest Circumpolar Deep Water of the western Atlantic to reestablish the saltier mean characteristics of the Pacific sector. A detailed description of the eastward progression in the characteristics of AABW through the Indian sector of the ACC is given in Section 3.1.

The mean characteristics of the AABW ($\gamma^n > 28.27$ kg m^{-3}) found in each sector of the ACC (Fig. 5) are more distinct than those for the Lower Circumpolar Deep Water immediately above ($28.18 < \gamma^n < 28.27$ kg m^{-3}). A divergence in the deep temperature–salinity curves, say at temperatures of about 0.3°C, was already noted for stations located farther to the south of the ACC near the slope (see Fig. 3(b)). Indeed, lateral mixing must be hindered at deeper isopycnals within the AABW: the bottom γ^n distribution (Fig. 2) demonstrates that eastward flow of AABW underneath the ACC is effectively blocked by the Mid-Atlantic Ridge (10°W, 50°S), Southwest

Indian Ridge (40°E, 45°S), the Kerguelen Plateau (75°E, 55°S), and the Southeast Indian Ridge (145°E, 55°S). No AABW is found in the ACC domain over the Agulhas, South Australian, and Southwest Pacific basins (see Fig. 1(b) for place names). But, deep property distributions indicate cyclonic circulations of Weddell Sea Deep Water underneath the ACC in the Scotia, Georgia and Enderby basins, and of mixtures of bottom waters formed off the Wilkes Land and Ross Sea in the Australian–Antarctic and eastern Southeast Pacific basins.

2.4. ACC Bottom Water

Within the density layer encompassing the deep salinity maximum (*S*-max)—the most prominent signal of the NADW—changes similar in magnitude to the AABW layer are observed, but in the opposite eastward progression along the ACC, are observed (Fig. 5). This northern signal is the strongest at its entry point into the circumpolar flow regime in the southwestern corner of the Argentine Basin, where it appears with $\theta > 2$°C and $S > 34.78$. A pronounced downstream freshening (and cooling on isopycnals) of the *S*-max is observed along the eastward passage of NADW through the Indian and Pacific sectors. Such a change is expected since NADW remnants constantly mix with less saline waters above and below and there is no additional salty inflow from the north or the south in any of those ocean sectors. This portion of the standard-deviation envelopes overlap for adjacent sectors since it can continue to flow unobstructed around the globe, unlike the denser AABW types—water near the deep salinity maximum are not topographically constricted to circulate within particular basins.

At certain locations the ACC extends close to the Antarctic continental margins (Fig. 1(a)). There CDW found at levels near the *S*-max (LCDW) is able to mix laterally with low-salinity mixtures of near-freezing subsurface waters. A dramatic freshening of LCDW is clear in the Atlantic sector of the ACC (Fig. 5). The Atlantic standard-deviation envelope not only shows the largest width near the *S*-max, but its is also fresher than the Pacific envelope. Such freshening results from significant northward export of Shelf Water mixtures from the Weddell–Scotia Confluence into the southern ACC (Whitworth, Nowlin, Orsi, Locarnini & Smith, 1994).

Perhaps the most remarkable feature in Fig. 5 is the hour-glass shape of these regional envelopes: within the CDW of the ACC is a clear density layer ($28.18 < \gamma^n < 28.27$ kg m^{-3}) with minimum scatter indicating that it is the most well-mixed product of the NADW above and the AABW below. This mixing takes place over many circuits around Antarctica, hence this water mass is likely to be the oldest within the ACC at levels below the salinity maximum, and thus it ought to be clearly identified on vertical sections by a deep CFC-minimum. The latter can be seen across the ACC on sections at 140°E, see Figs. 2(b) and (e) in Rintoul and Bullister (1999), and at Drake Passage, see Figs. 2(a–b) of Roether, Schlitzer, Putzka, Beining, Bulsiewicz et al. (1993): the deep CFC-11 minimum lies about 1000 m below the *S*-max in both sections.

Because this dense portion of the ACC's CDW is not directly advected into the ACC from the north (see Fig. 2) and because its spatial distribution is indeed circum-

polar, we will call it 'ACC Bottom Water' (ACCbw). ACCbw is the least spatially variable water mass of the circumpolar current. Thus, the southern bottom water in Fig. 2 is composed of AABW (blue dots) and ACCbw (red dots). As discussed in Section 2.1, ACCbw is the only southern bottom water exported in all the western boundary currents of the Southern Hemisphere. It is replenished from underneath by upwelling of AABW, as well as laterally from the south by volumes of equally dense mixtures, called Modified Circumpolar Deep Water (MCDW), formed over the Antarctic shelf-slope regime (Whitworth et al., 1998).

3. Southern Ocean circulation

Next is the first global description of the AABW circulation based on the topography of $\gamma^n = 28.27\ \mathrm{kg\ m^{-3}}$ (Fig. 6), the bottom layer depth-averaged CFC-11 distri-

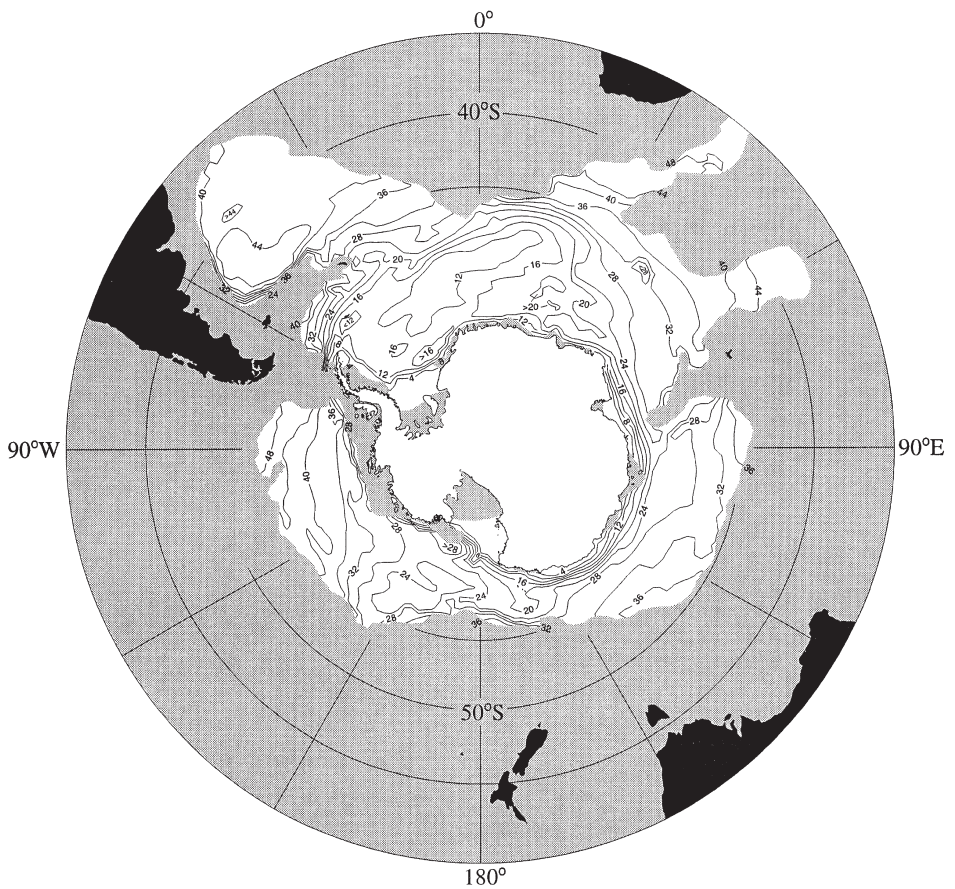

Fig. 6. Depth (hm) of $\gamma^n = 28.27\ \mathrm{kg\ m^{-3}}$, the neutral density surface defining the top of Antarctic Bottom Water.

bution (Fig. 7(a)), and similar maps of AABW potential temperature, salinity and thickness (Fig. 7(b–d)). A schematic of the inferred flow pattern of different density constituents within the AABW layer is presented in Fig. 7(e). Fields shown in Figs. 6 and 7(a–d) were used in the computation of the AABW volumetric characteristics of Section 3.3, and in the global production rate estimates of Section 5. Because CFC-11 measurements were taken over the 1984–1996 period, they were normalized to different mid-term years (1987 in the Atlantic and 1993 in the Indian–Pacific sectors) to minimize the temporal biasing inherent to the sampling. Except for the hand-contoured map in Fig. 7(a), all station data shown in Fig. 1(a) have been objectively mapped (Roemmich, 1983) to a polar stereographic grid for the area south of 30°S (Fig. 1(b)), adopting a Gaussian covariance with correlation length scales of 850 km and 350 km in the zonal and meridional directions. The objective mapping smooths out smaller-scale features, and the mean property maps shown here (Fig.

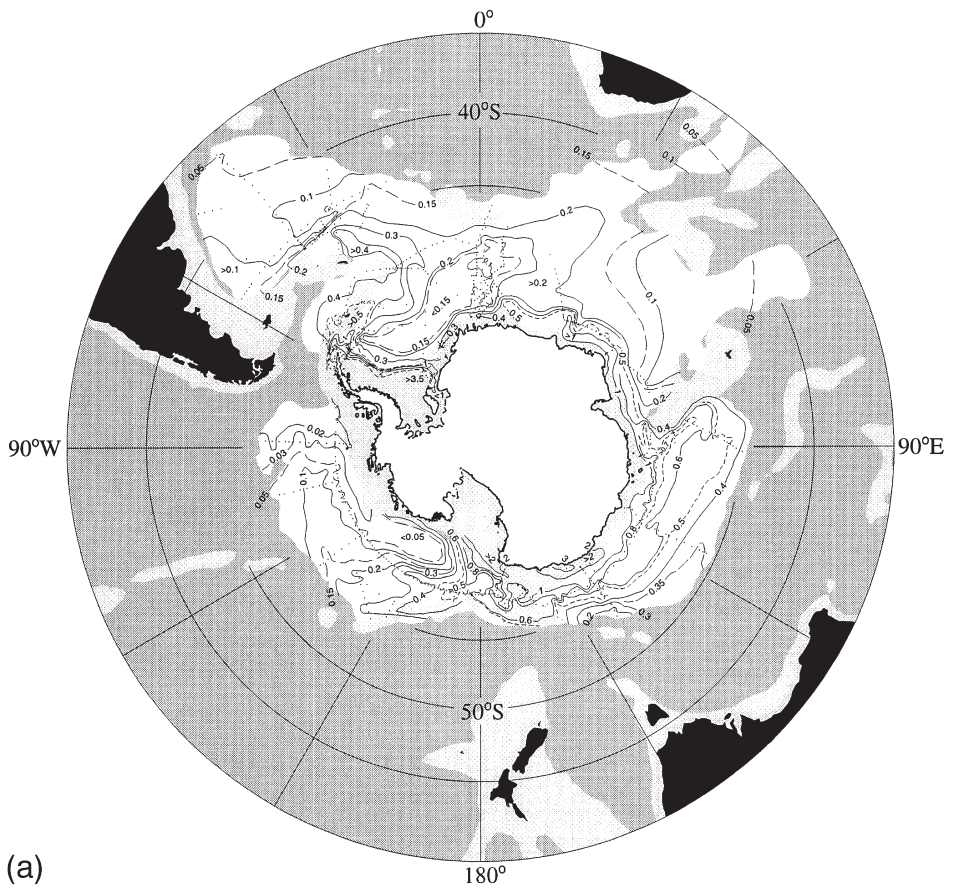

Fig. 7. Distribution of mean (depth-averaged) properties of the Antarctic Bottom Water layer: (a) CFC-11 (pmol kg^{-1}).

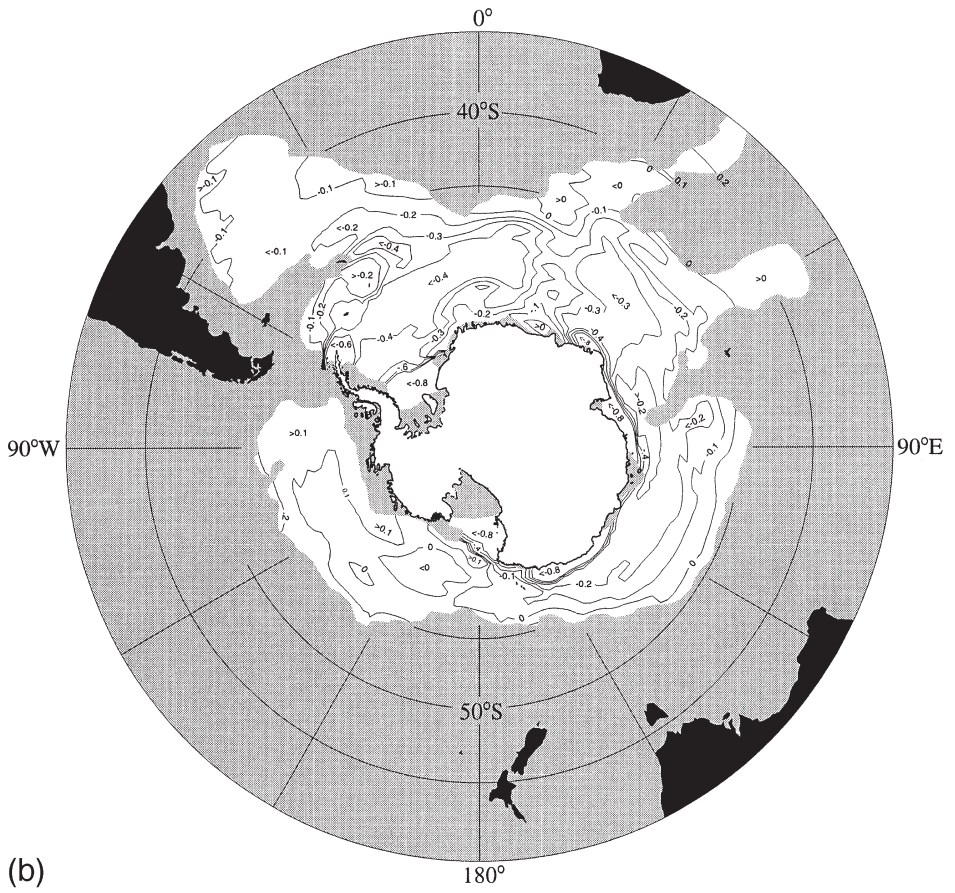

Fig. 7. Distribution of mean (depth-averaged) properties of the Antarctic Bottom Water layer: (b) potential temperature (°C).

7(b–d)) only depict the large-scale patterns of AABW that are prominent enough to survive this approach; thus, they are not meant to reveal previously undocumented circulation features. More detailed bottom and isopycnal maps are available in the Antarctic literature, especially from more regional studies of each of the various AABW components discussed in Section 2.1 (Carmack, 1977; Mantyla & Reid, 1983, 1995; Orsi et al., 1993; Gordon, 1998; Locarnini, 1994).

The $\gamma^n = 28.27$ kg m^{-3} isopycnal lies at its shallowest ($Z < 400$ m) at the sites over the continental margins where the densest AABW types are formed (Fig. 6). There, newly-formed bottom water is adjacent to near-freezing Shelf Water (see Fig. 12 in Whitworth et al., 1998) whose recent exposure to the atmosphere accounts for the highest CFC concentrations (CFC-11 > 1 pmol kg^{-1}, Fig. 7(a)) and lowest potential temperatures ($\theta < -0.8$°C, Fig. 7(b)) within the entire AABW layer. This situation is indicated schematically by the solid arrows in Fig. 7(e), which represent

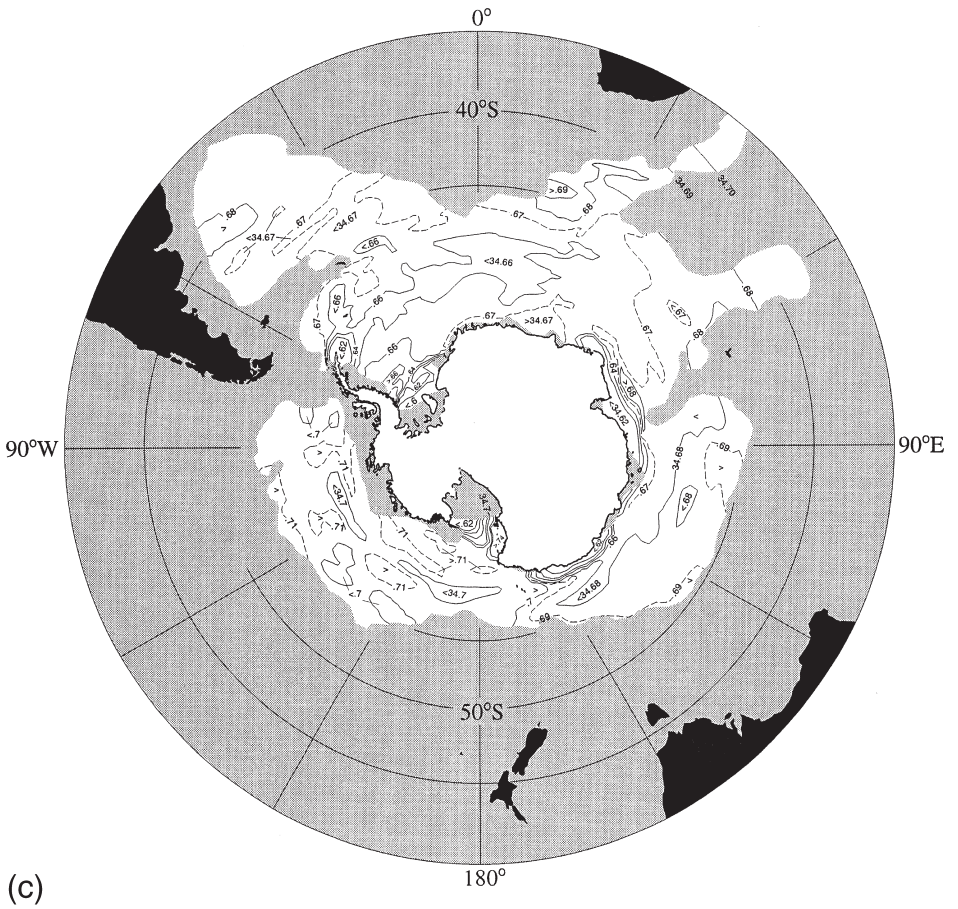

Fig. 7. Distribution of mean (depth-averaged) properties of the Antarctic Bottom Water layer: (c) salinity.

newly formed bottom waters sinking downslope over the western Weddell Sea (60°–30°W), around the Amery Basin (50°–100°E), Wilkes Land (120°–160°E), and the Ross Sea (170°E–160°W). The last source region is the only one to show a marked salinity gradient, which is nearly aligned on the date line (Fig. 7(c)) and separates low-salinity Shelf Water to the east ($S < 34.70$) from high-salinity Shelf Water to the west. At locations where there is neither Shelf Water nor its cold derivatives over the shelves, the $\gamma^n = 28.27\ \mathrm{kg\ m^{-3}}$ isopycnal intersects the ocean floor at mid to great depths along the Antarctic continental slope: over the eastern Weddell Sea and in the western Australian–Antarctic and eastern Southeast Pacific basins. Hence at all these locations the waters occupying the shelf-slope regime are not dense enough to sink underneath the Circumpolar Deep Water circulating offshore (Whitworth et al., 1998).

Westward flow along the continental slopes of newly-formed AABW types is

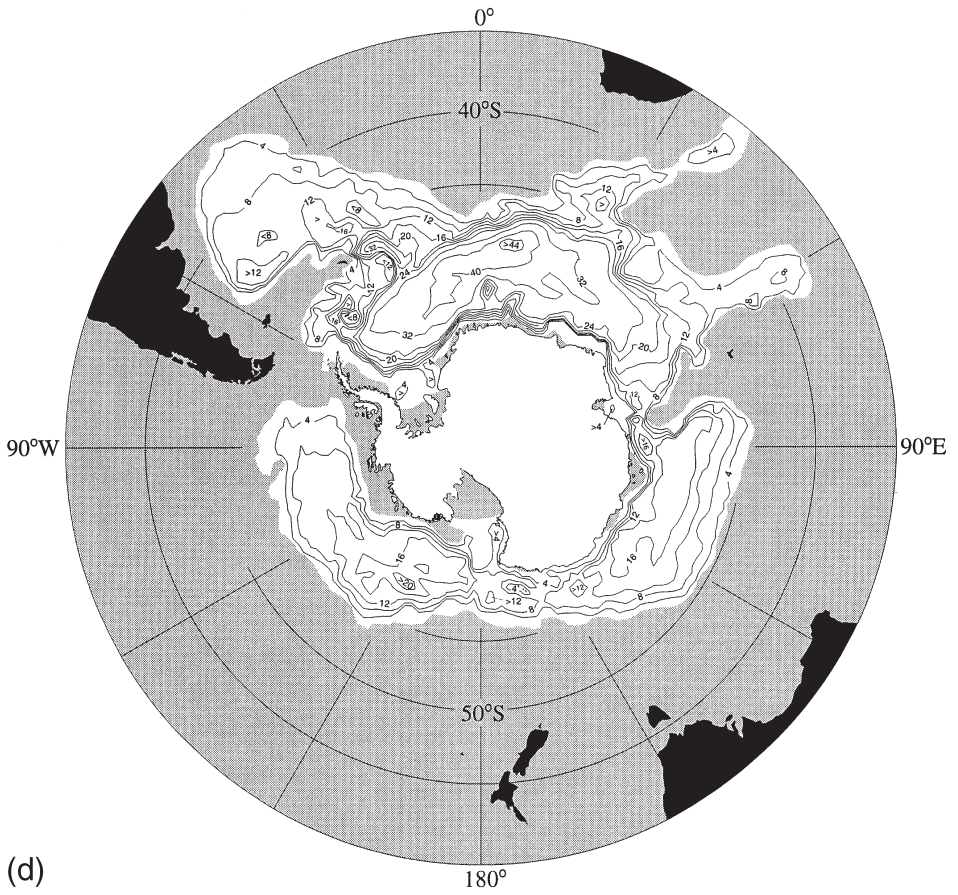

Fig. 7. Distribution of mean (depth-averaged) properties of the Antarctic Bottom Water layer: (d) thickness (hm) of the water column beneath $\gamma^n = 28.27\ kg\ m^{-3}$, i.e. the Antarctic Bottom Water thickness.

implied in all three Antarctic basins. Upon spilling over the shelf break, young bottom waters produce conspicuously high-CFC-11 signals (Fig. 7(a)) that are clearly traceable to their corresponding shallower source regions (see solid arrows in Fig. 7(e)). The steep seaward deepening of $\gamma^n = 28.27\ kg\ m^{-3}$ from the Shelf Water domains (Fig. 6) indicates local westward flow of AABW relative to a shallower reference level over the slope regime. Salty Ross Sea Bottom Water with $S > 34.7$ (Fig. 7(c)) and mean CFC-11 > 1.5 pmol kg^{-1} (Fig. 7(a)) spreads between the Balleny Ridge and the Antarctic slope toward the southeastern corner of the Australian–Antarctic Basin. Low salinity Adélie Land Bottom Water ($S < 34.68$) extends to the west of 140°E has even higher concentrations (CFC-11 > 2 pmol kg^{-1}). A high-CFC signal (CFC-11 > 1 pmol kg^{-1}) in the new low-salinity ($S < 34.64$) bottom water type formed near the Amery Basin (Carmack & Foster, 1975; Jacobs & Georgi, 1977) reaches as far west as 25°W still with CFC-11 > 0.3 pmol kg^{-1}. Just west of

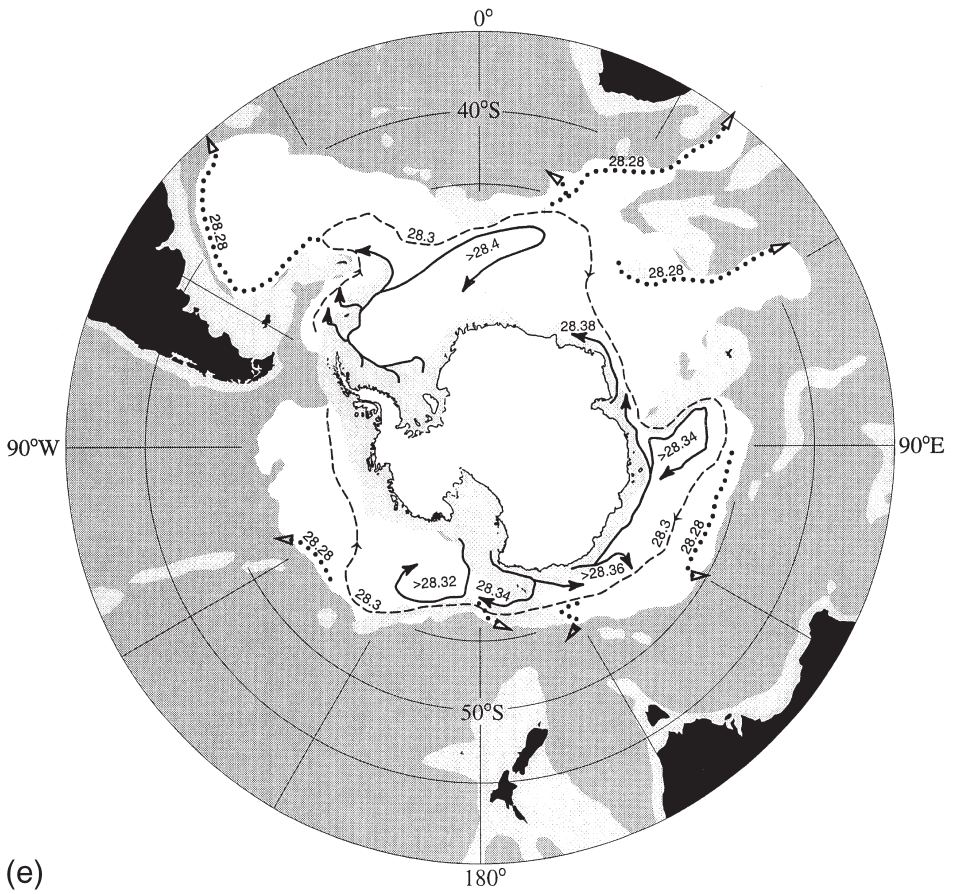

Fig. 7. Distribution of mean (depth-averaged) properties of the Antarctic Bottom Water layer: (e) schematic flow pattern of AABW components with different density values, as indicated by the labels.

30°W, this eastern signal is locally reinforced by an even stronger CFC (CFC-11 > 3 pmol kg^{-1}) and low-salinity ($S < 34.62$) signal, from newly-formed Weddell Sea Bottom Water spilling off the Filchner Depression (Schlosser, Bullister & Bayer, 1991; Mensch, Bayer, Bullister, Schlosser & Weiss, 1997).

Once it has reached the oceanic domain, AABW participates in the cyclonic circulations of the major Subpolar gyres (Fig. 7(e)). In the northwestern corner of the Weddell Sea young Weddell Sea Bottom Water with mean $S < 34.66$, $\theta < -0.4$°C and CFC-11 > 0.5 pmol kg^{-1} leaves the slope regime (Fahrbach et al., 1995; Muench & Gordon, 1995) and flows cyclonically along the northern limb of the Weddell Gyre (Orsi et al., 1993). This clockwise circulation is clearly indicated, relative to a deeper reference level, by the large doming of $\gamma^n = 28.27$ kg m^{-3} (Fig. 6; $Z < 1600$ m). Similarly, the relatively more ventilated (CFC-11 > 0.6 pmol kg^{-1}) low-salinity ($S < 34.68$) AABW formed off Wilkes Land flows cyclonically along

the southern and western rims of the Australian–Antarctic Basin (Mantyla & Reid, 1995; Orsi & Bullister, 1996). A clockwise loop in the last high-CFC signal (Fig. 7(a)) clearly wraps around the tight dome in the relief of $\gamma^n = 28.27\ kg\ m^{-3}$ (Fig. 6) just to the east of the Kerguelen Plateau. An elongated center is indicated for the Ross Gyre cyclonic circulation (Fig. 6); it trends from around the Balleny Islands to the northeast and it includes at least the two small dome-like interior cells where $\gamma^n = 28.27\ kg\ m^{-3}$ is shallower than 2400 m (and the layer-mean $\theta < 0°C$). Two high-CFC lobes are found within the gyre's interior, one along the offshore deeper branch of salty Ross Sea Bottom Water, which is pressed against the western flank of the Balleny Ridge (CFC-11 > 1 pmol kg^{-1}), and the other along the low-salinity Ross Sea Bottom Water, which is spreading to the north along 175°W (CFC-11 > 0.6 pmol kg^{-1}).

Some AABW flows eastward following the path of the ACC waters above (see Fig. 7(e); dashed line), which is marked in Fig. 6 by the pronounced equatorward descent of $\gamma^n = 28.27\ kg\ m^{-3}$ from depths of about 2200 m to near 4000 m. Thus, a portion of the Weddell Sea Deep Water exported at the northeastern end of Weddell Gyre continues to flow eastward into the Enderby Basin to as far east as 60°E with a relatively low mean temperature (− 0.3°C), salinity (34.67), and high CFC-11 concentration (0.15 pmol kg^{-1}). At this location the bottom layer of AABW is still about 2000 m thick.

3.1. Interbasin sills

Farther downstream there is a rapid thinning of the AABW layer over the sill of the passage between the Kerguelen Plateau (75°E, 55°S) and the Antarctic coast to less than 1200 m; and then again between the Pacific–Antarctic Ridge (160°E, 60°S) and the Balleny Islands, to less than 800 m. These are the two major choke points which hinder the eastward exchange of AABW between the Antarctic basins, namely (see Fig. 1) the sill of the Princess Elizabeth Trough located near 80°E and 65°S, and the sill located near 160°E and 65°S, hereafter referred to as the Balleny Trough. Despite this thinning, using the bottom as the reference, nearly 1.5 Sv of AABW (i.e. Weddell Sea Deep Water) from the Enderby Basin enters the Australian–Antarctic Basin across the northern half of the 80°E section of Speer and Forbes (1994). Computing across two 170°E sections, the Eltanin section in Gordon (1975) and the preliminary WOCE P14S line in Orsi and Bullister (1996), gives estimates of about one fifth of that volume continuing eastward below $\gamma^n = 28.27\ kg\ m^{-3}$ into the northern limb of the Ross Gyre through the Balleny Trough.

Gordon (1975) suggested that Weddell Sea Deep Water from the northern limb of the Weddell Gyre could end up as far east as 170°E, within the northern limb of the Ross Gyre, and the global description of Carmack (1977) also supported this notion. This long quasi-circumpolar route linking AABW (with $\gamma^n \approx 28.3\ kg\ m^{-3}$) of the Scotia with that of the Bellingshausen seas is indicated schematically by the dashed line in Fig. 7(e). The coldest bottom temperatures observed over the two major sills are about − 0.4°C (and $\gamma^n = 28.35\ kg\ m^{-3}$) over the Princess Elizabeth Trough, and − 0.2°C (and $\gamma^n = 28.34\ kg\ m^{-3}$) over the Balleny Trough (Carmack,

1977). This last eastward increase of the sill temperatures is also evident in Fig. 5 from the temperature at which the deep envelopes diverge.

The salinity field reveals that there is eastward export of relatively fresh ($S < 34.69$) AABW into the Southeast Pacific Basin across the northern half of the Balleny Trough (Fig. 7(c)), immediately to the north of the salty input coming from the western Ross Sea into the eastern Australian–Antarctic Basin. The cyclonic circulation of the Ross Gyre carries this deep low salinity signal farther eastwards, along its northern limb. Indian AABW shows up as a clear deep salinity minimum on vertical distributions at 170°E in Gordon (1975) and at 170°W in Reid (1990): it is wedged between the saltier ACCbw above and the underlying high-salinity Ross Sea Bottom Water. These two saline influences are predominant in determining the mean salinity ($S > 34.71$) of the Southeast Pacific Basin bottom layer, which is the saltiest in Fig. 7(c) (see also Fig. 5).

3.2. Deep water mixing in the Southern Indian Ocean

Properties of the AABW that follow the long eastward path through the three Antarctic basins ought to reflect influences from any other local source of deep and bottom waters encountered along the way. Orsi et al. (1995) defined the southernmost front and boundary of the ACC based on water mass properties and geostrophic shear in the Southern Ocean. Stations located along this southern band of the ACC (Fig. 8(a)) were averaged in longitude-sectors to compute their mean characteristic relationships on a series of neutral density horizons (Fig. 8(b)). Regional changes in the AABW characteristics are revealed by the downstream sequence of average θ–S curves observed along the poleward fringes of the ACC.

Relatively fresh Weddell Sea Deep Water (•'s) with $-0.2°C < \theta < -0.4°C$ (Fig. 8(b)) becomes progressively saltier as it enters the Australian–Antarctic Basin (+ 's), where most of the AABW layer shows nearly uniform salinities (about 34.68 at $\theta < -0.2°C$) between 90°E and 150°E (△'s and × 's). In contrast, a rapid salinification of AABW occurs for $\theta < -0.1°C$ at the eastern end of that basin (○'s), with maximum increase near the bottom reflecting the input of high-salinity bottom water from the Ross Sea (Gordon & Tchernia, 1972; Rintoul, 1998). This branching of deep characteristic curves has been used here to distinguish deep waters with sources located at different Antarctic shelves (Rodman & Gordon, 1982; Speer & Forbes, 1994). Since waters colder than $-0.4°C$ do not flow over the Princess Elizabeth Trough, a local source of low-salinity bottom water must exist along the shelves of the Australian–Antarctic Basin to compensate for the salty influx from the Pacific sector. Moreover, local (Indian) sources of low-salinity *deep* water are required to explain the relatively fresh mean curve for the 60°–90°E sector (+'s) at $-0.2°C < \theta < 0.5°C$. Thus, both the top portion of the AABW and most of the ACCbw ($28.18 < \gamma^n < 28.27$ kg m^{-3}) must mix substantially as they pass through this sector. Lateral mixing with equally dense Shelf Water mixtures exported off the local continental margins (85°–95°E), is facilitated by the cyclonic circulation inferred over the southwestern Australian–Antarctic Basin (Figs. 6 and 7); the low-salinity signal is then carried northward by the Deep Western Boundary Current

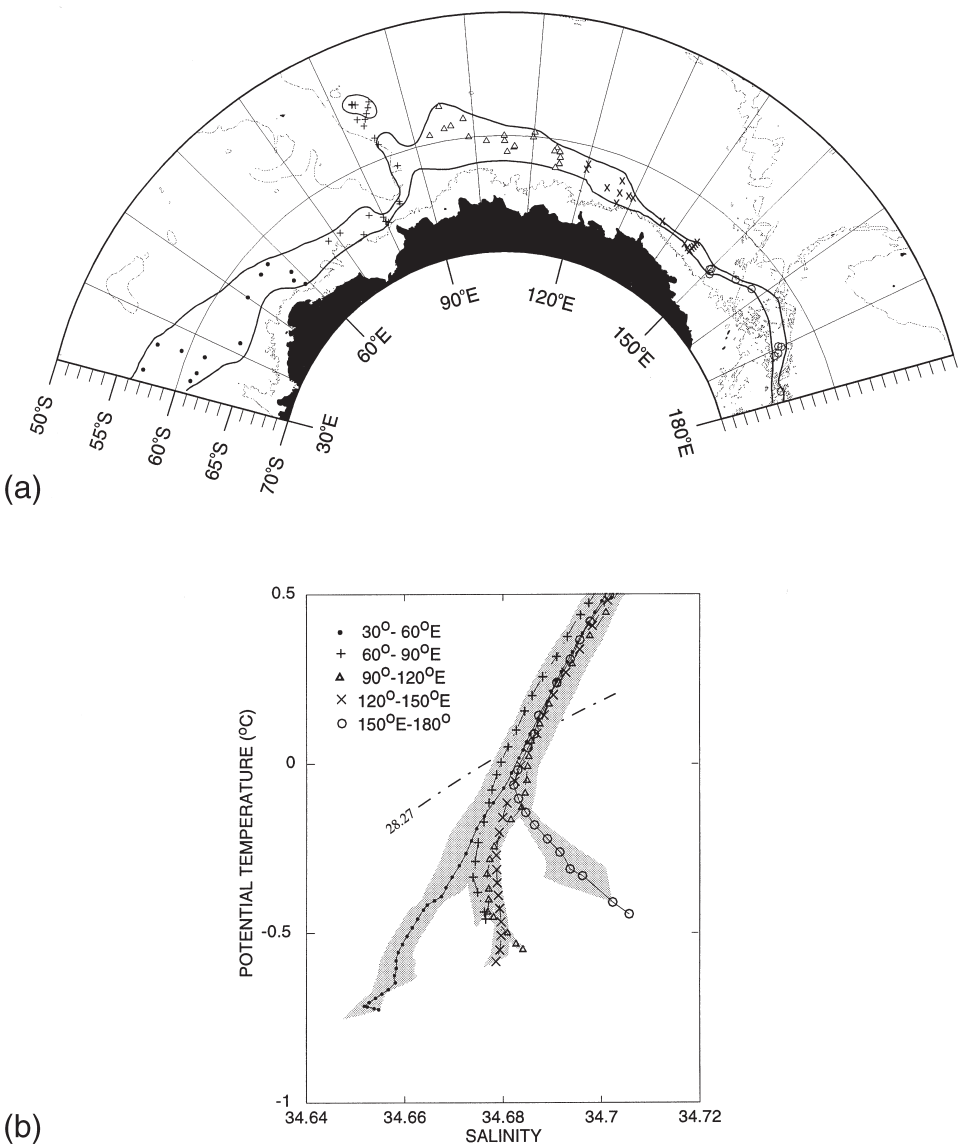

Fig. 8. (a) Top: Distribution of selected stations located within 30°-longitude bins along the southernmost water-mass zone of the Antarctic Circumpolar Current, i.e. stations that are bounded by the poleward boundary and the southern front of the Antarctic Circumpolar Current, as in Orsi et al. (1995), which are indicated by the heavy solid lines. Symbols are used to distinguish stations from different bins, and the thin line is the 2500-m isobath. (b) Bottom: Mean characteristic θ–S diagrams for deep waters in each longitude-bin shown in (a) are indicated by solid curves connecting: dots (•) for the 30°–60°E bin, pluses (+) for the 60°–90°E, triangles (Δ) for the 90°–120°E, crosses (×) for the 120°–150°E, and circles (○) for the 150°E–180°. Shaded behind these mean curves are the one standard error envelopes of the mean curves, all computed at a preselected set of neutral density surfaces. The dot-dashed line indicates $\gamma^n = 28.27$ kg m^{-3}.

observed against the eastern flank of the Kerguelen Plateau (Tchernia & Jeannin, 1983; Speer & Forbes, 1994; Orsi et al., 1995).

3.3. Deep water ventilation in the Australian–Antarctic Basin

To reveal more peculiarities of the deep waters of Australian–Antarctic Basin, we compare its volume-weighted average properties (θ, S and CFC-11) with those of the adjacent basins. We used the information from all fields presented in Figs. 6 and 7, in combination with the corresponding areal information, and the two controlling sill depths—at the Princess Elizabeth Trough (80°E) and the Balleny Trough (160°E)—to divide these results into three major basin systems as shown in Table 2. Thus, in this work the Atlantic sector includes the Weddell–Enderby, Georgia, and Argentine basins with portions of the Drake Passage, and the Scotia, Agulhas, and Crozet basins; whereas the Indian and Pacific sectors only include the Australian–Antarctic and Southeast Pacific basins, respectively. The volume of AABW in all these basins combined is only about 3.5% of the World Ocean's volume, and it covers only about 9% of the sea floor. However its low mean temperature of −0.23°C makes the AABW an important component of the ocean's climate.

As shown above, the volumes of AABW residing within the abyssal domains of these basins (Fig. 7(e)) blend in the multiple signals carried by well-ventilated deep and bottom waters spreading away from their shallower sources, before they slowly move upward into the layer above to feed the western boundary currents carrying AACbw—the bottom branches indicated by the red dots in Fig. 2. Considerable entrainment of less dense and older environment waters (CDW) occurs as these young waters leave the shelf domain and sink down the slope, thus to include the bulk of such volume gain in our volumetric census (and production rate estimates given in Section 5) we start our computations at the 2500-m isobath over the slope, and end equatorward where $\gamma^n = 28.27\ \mathrm{kg\ m^{-3}}$ intersects the ocean floor.

There are conspicuous property differences in the characteristics of AABW of the three Antarctic sectors, as has already been pointed out above in the study of the

Table 2
Mean characteristics of Antarctic Bottom Water

Ocean sector	Volume-weighted averages						
	Area (10^3 km^2)	%	Volume (10^3 km^3)	%	Pot. temp. $\overline{\theta}$ (°C)	Salinity $\overline{S}$	CFC-11 (pmol kg^{-1})
Atlantic 70°W–80°E	19 814	61	33 861	71	−0.30	34.66	0.17 (norm. 1987)
Indian 80°–160°E	5771	17	6856	14	−0.17	34.68	0.47 (norm. 1993)
Pacific 160°E–70°W	7059	22	7263	15	0.04	34.71	0.18 (norm. 1993)
Total	32 644		47 980		−0.23	34.67	0.22

volumes of AABW lying underneath the ACC (Fig. 5). Similarly, based on the volumetric averages presented here, both temperatures and salinities increase progressively to the east from the Weddell–Enderby ($\bar{\theta} = -0.3$°C, $\bar{S} = 34.66$) to the Southeast Pacific basins ($\bar{\theta} = 0.04$°C, $\bar{S} = 34.71$). AABW of the Indian basin displays intermediate mean temperature and salinity values ($\bar{\theta} = -0.17$°C, $\bar{S} = 34.68$) as a result of the multiple inputs from the local low-salinity sources of bottom and deep waters with $\gamma^n > 28.27$ kg m^{-3} located along the Wilkes Land (120°–160°E).

Special consideration was given to the computation of the average CFC-11 concentrations presented in Table 2, toward reducing the temporal bias of these transient tracer measurements available from these basins (see Fig. 7(a)). Most of the CFC data from the Atlantic sector were collected from about 1984–1990, so they have been normalized to 1987; whereas most of those from the Indian and Pacific sectors span 1991–1996, and have been normalized to 1993. The average change in atmospheric CFC concentrations in the southern hemisphere was about 2–3% per year during these time intervals. If dissolved CFCs in Shelf Water are assumed to track the atmospheric trends (Schlosser et al., 1991), then a temporal bias towards values 18% higher might be expected for CFCs in newly formed bottom waters in the Indian and Pacific sectors relative to the Atlantic sector. However, mean (normalized) CFC-11 concentration in the Antarctic–Australian Basin (0.47 pmol kg^{-1}) are approximately double those in the adjacent (Weddell–Enderby and Southeast Pacific) basins; thus, such a high-CFC signal must be associated with the local formation of bottom waters along the southern margins of this basin.

A vigorous production of recently ventilated deep and bottom waters and/or a relatively short residence time within the Australian–Antarctic Basin is suggested by the high CFC-11 concentration of its AABW layer. Although the Indian and Pacific sectors contain about the same volume of AABW, one can argue from the (limited) data set shown in Fig. 7(a) that the Southeast Pacific Basin is the more poorly ventilated. This may result in part from the Balleny Trough effectively blocking the eastward passage of the densest bottom water in the Australian–Antarctic Basin. Thus the circulation near the northwestern end of the Ross Gyre facilitates the ventilation of the Australian–Antarctic Basin by exporting Ross Sea Bottom Water and deep waters formed along the coast of Victoria Land (150°–170°E) to the west. This is in a remarkable contrast with the Weddell Gyre's contribution to the bottom layer of the Southeast Pacific Basin, which is negligible west of Drake Passage.

Caution must be exercised while interpreting the mean characteristics of the AABW filling these subpolar basins in relation to the uncertain strengths of the multiple contributing sources of deep and bottom waters formed around Antarctica. That problem is considered in Section 5, but it is commonly thought that the sources in the Weddell Sea are the most productive. Our mean property maps reflect at least one distinctive feature of the Weddell–Enderby varieties of AABW: they are the only ones free to communicate directly and ventilate the abyssal basins located farther to the north. These equatorward exports from the Weddell Gyre are indicated schematically by the dotted lines in Fig. 7(e). Even though the northern ridges bounding all three Antarctic basins have about the same sill depth (Fig. 1), as well as deep gaps, those in the eastern Indian and Pacific sectors effectively block any outflow

of AABW. The AABW varieties of the Antarctic–Australian and Southeast Pacific basins, say with $\gamma^n = 28.27$–$28.28\ kg\ m^{-3}$ (Fig. 7(e); dotted lines), have to be entrained into the ACCbw layer before being able to continue further north along the corresponding abyssal Western Boundary Currents.

4. South Atlantic ventilation

All of the measured CFC concentrations in the ocean interior are ultimately derived from the atmosphere; the bulk of it via sea-surface gas exchange. The atmospheric signal is imprinted where isopycnals outcrop and thence carried into the ocean interior, where it can be used to trace the pathways followed by water masses and to estimate their ventilation rates (Warner & Weiss, 1992; Doney & Bullister, 1992). CFC concentrations are usually highest in near-surface waters so vertical diffusion can also contribute to the mixing of CFCs down into the interior of the deep ocean. In the abyssal Southern Ocean, however, there is no such net flux of CFC from the overlying relatively old and CFC-poor ACCbw into the more vigorously ventilated CFC-rich AABW.

Dense waters are exported northward from the Weddell Sea along two routes (Gordon, 1966; Locarnini et al., 1993): some Weddell Sea Deep Water ($-0.7°C < \theta < 0°C$) overflows the South Scotia Ridge (Nowlin & Zenk, 1988) before continuing eastward along the southern Scotia Sea, but another component branches to the north along the South Sandwich Trench above the colder Weddell Sea Bottom water ($\theta < -0.7°C$; Reid et al., 1977). Next we will illustrate these routes and the circulation of AABW varieties within the Weddell Gyre using the available transient tracer measurements (CFC-11) in the South Atlantic (Fig. 9). The discussion starts with the section (Fig. 10) closest to the sources of Weddell Sea Bottom Water, the AJAX line (SIO/TAMU, 1985; Weiss, Bullister, Warner, Van Woy & Salameh, 1990) located (Fig. 9) across the South Sandwich Island Arc, which spans the southern edge of the ACC and the northern limb of the Weddell Gyre.

4.1. Weddell Sea deep and intermediate water outflows

Relatively new Weddell Sea Bottom Water is carried eastward from the northwestern Weddell Basin by a northern boundary current banked against the South Scotia Ridge (Bullister, 1989). Part of this flow splits near 25°W, 60°S (see Fig. 2 of Locarnini et al., 1993) where the bottom ridges also seem to diverge. As indicated by the CFC-11 distribution (Fig. 7(a)), some Weddell Sea Bottom Water peals off to the north to fill the bottom layer of the South Sandwich Trench and Georgia Basin (Gordon, 1966, 1967), whereas the rest continues eastward to flow cyclonically within the Weddell Basin (Orsi et al., 1993). Thus in Fig. 10, for $\gamma^n > 28.40\ kg\ m^{-3}$ ($\sigma_4 \gtrsim 46.16\ kg\ m^{-3}$) there are two cores with the highest concentrations (CFC-11 > $0.4\ pmol\ kg^{-1}$): one located over the western side of the South Sandwich Trench and the other pressed against the southern flank of the America–Antarctic Ridge. All deep waters of interest show relatively small variations in temperature and salinity,

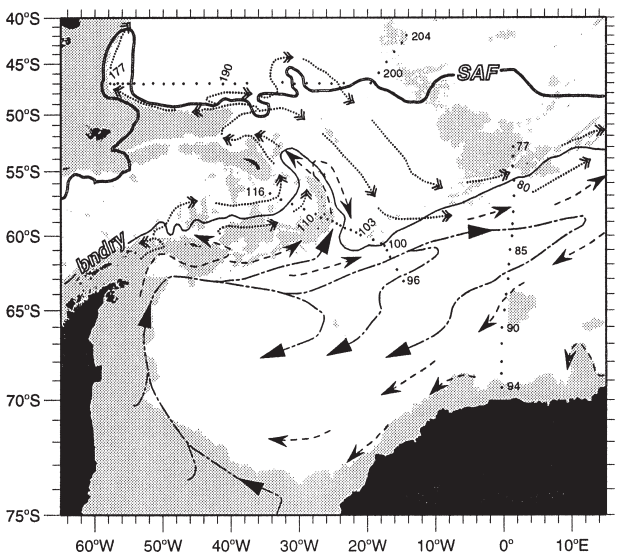

Fig. 9. Map of the western South Atlantic showing the station locations of the AJAX (116-96 and 77-94) and SAVE (171-205) hydrographic lines; the traces of the Subantarctic Front (SAF) and southern boundary (bndry) of the Antarctic Circumpolar Currents are included, from Orsi et al. (1995). Distinct line types, and arrow-heads, indicate the schematic flow pattern at the bottom as followed by Weddell Sea waters with different densities: dot-dashed for $\gamma^n > 28.42\ kg\ m^{-3}$, dashed for $28.35 < \gamma^n < 28.42\ kg\ m^{-3}$, and dotted for $28.27 < \gamma^n < 28.35\ kg\ m^{-3}$.

so their CFC-11 solubility coefficients are essentially constant. Therefore, at least quantitatively, the latter bottom CFC-11 maxima (Fig. 10(b)) are also comparable to minima in pCFC-apparent age (Doney & Bullister, 1992). Further evidence that these bottom signals (CFC-11 maxima) are representative of the youngest outflowing bottom waters is found in their being the most oxygen-rich ($O_2 > 250\ \mu mol\ kg^{-1}$), the coldest ($\theta < -0.7°C$), the freshest ($S < 34.65$) and the most silica-poor ($H_2SiO_4 < 125\ \mu mol\ kg^{-1}$), all characteristics of recently-formed Weddell Sea Bottom Water.

Elevated levels of CFC in bottom waters ($0.3 <$ CFC-11 $< 0.4\ pmol\ kg^{-1}$) are also observed in the Scotia Sea (stas. 116–112), although this water is relatively warm ($-0.4°C < \theta < 0°C$) and light ($\gamma^n < 28.34\ kg\ m^{-3}$; $\sigma_2 \lesssim 37.19\ kg\ m^{-3}$) compared to Weddell Sea Bottom Water. Weddell Sea Deep Water escapes from the Weddell Basin via deep gaps in, and over, the South Scotia Ridge (Nowlin & Zenk, 1988). This water is an important component of the northward outflow into the abyssal layers of the Georgia and Argentine basins, which reinforces the one carried out along the South Sandwich Trench route (Locarnini et al., 1993). Both outflows meet in the Georgia Basin before continuing northward into the Argentine Basin (Fig. 9). Yet, most of the relatively cold Weddell Sea Deep Water of the Georgia Basin ($\theta < -0.5°C$) returns poleward south of the Falkland Ridge and west of the Islas Orcadas Rise, following the main path of the southern ACC front and boundary (Orsi et al., 1993; Locarnini et al., 1993).

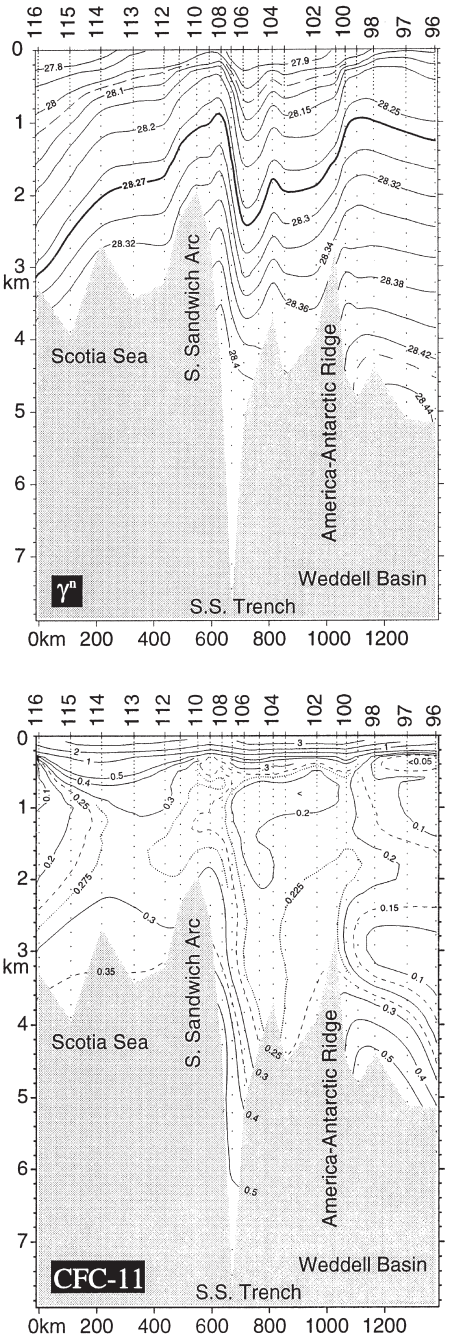

Fig. 10. Neutral density γ^n (kg m^{-3}) and CFC-11 (pmol kg^{-1}) along the AJAX section of 1984 extending southeastward across the South Sandwich system. See Fig. 9 for section location.

As reflected (Fig. 9) by the trace of the southern boundary of the ACC (bndry), the Weddell Gyre's northern limb turns equatorward around the South Sandwich Islands Arc, followed by a poleward loop of the ACC just to the east. Therefore the southern boundary of the ACC crosses this AJAX section three times: twice northeastward (between stas. 115–114 and again between stas. 101–100), and once southwestward (between stas. 107–106). Less well ventilated (CFC-11 $<$ 0.2 pmol kg^{-1}) Circumpolar Deep Water carried along the southern edges of the ACC is seen for $\gamma^n < 28.27$ kg m^{-3} ($\sigma_2 \lesssim 37.16$ kg m^{-3}) at stas 116, 115, and 106–101 in Fig. 10(b). Even lower CFC concentrations are observed in the interior of the Weddell Gyre at stas. 99–96 (CFC-11 $<$ 0.05 pmol kg^{-1}), where the water consists of relatively older recirculating ACCbw ($28.18 < \gamma^n < 28.27$ kg m^{-3}) that was originally imported from the circumpolar current near the eastern end of the gyre (Orsi et al., 1993).

Eastward flows of relatively light Shelf Water mixtures from the northwestern Weddell Sea have been observed to carry a high-CFC signal along the Weddell–Scotia Confluence (Whitworth et al., 1994). Remnants of this anomalous thermohaline stratification are traced as far north as the southern Argentine Basin (Whitworth, Nowlin, Pillsbury, Moore & Weiss, 1991) and as far east as 22°E (Orsi et al., 1993). In Fig. 10(b) this direct lateral influence from the Antarctic margins is evident in the weakening of the CFC-minimum cores appearing conspicuously at stas. 114–111 (CFC-11 $>$ 0.25 pmol kg^{-1} near 1000–2000 m) and 100 (CFC-11 $>$ 0.2 pmol kg^{-1} near 400–1400 m). Both cores produce a distinctive maximum on isopycnal distributions of CFC within the density layer $\gamma^n = 28.15$–28.25 kg m^{-3} ($\sigma_0 \approx 27.82$–27.85 kg m^{-3}, $\sigma_2 \approx 37.08$–37.15 kg m^{-3}; see for instance Fig. 2 of Whitworth et al., 1994). Intermediate high-CFC signals like these are further evidence of the rapid lateral ventilation of Circumpolar Deep Water of the ACC by Weddell Sea waters in this particular region of the Southern Ocean.

Similarly, lateral ventilation also seems to affect the Weddell Sea Deep Water with $28.30 < \gamma_n < 28.34$ kg m^{-3} ($\sigma_2 \approx 37.17$–37.20 kg m^{-3}). This last influence is indicated by the relatively high concentrations seen along its anticlockwise return-loop beneath the ACC, i.e. by the CFC-11 $>$ 0.225 pmol kg^{-1} at stas. 103–101 (2000–4000 m) and along the northern limb of the Weddell Gyre by the CFC-11 $>$ 0.15 pmol kg^{-1} at stas. 100–96 (1600 m–2400 m).

4.2. Southern Argentine Basin

Whitworth et al. (1991) measured Weddell Sea Deep Water colder than $-$ 0.2°C entering the Argentine Basin from the Georgia Basin through a deep gap in the Falkland Ridge, near 36°W, 49°S (see their Fig. 2). This inflow supplies the abyssal western boundary current leaning against the Argentine continental slope, although part of it returns to the east via a very tight recirculation cell. The Subantarctic and Polar fronts of the ACC are often seen merged together as they extend eastwards along the northern flank of the Falkland Plateau east of about 46°W (Orsi et al., 1995). Both ACC fronts also coalesce while fluctuating meridionally over the deep gap in the Falkland Ridge (Peterson & Whitworth, 1989); a peculiar interaction

between the ACC and the local bathymetry that can either block or enhance the volume transport of Weddell Sea Deep Water into the Argentine Basin (Whitworth et al., 1991). The ventilation of the southern Argentine Basin by northward-flowing Weddell Sea Deep Water is examined here along an hydrographic section (Fig. 9) occupied in 1988 during the SAVE Expedition (Weiss, Warner, Salameh, Van Woy & Harrison, 1993).

Occasional, but rather rapid, northward fluctuations of the Subantarctic and Polar Fronts around the gap in the Falkland Ridge are expected to inject a clear high-CFC signal from the relatively cold Weddell Sea Deep Water of the Georgia Basin into the southern Argentine Basin (Whitworth et al., 1991). Part of that signal is then carried to the northwest by the abyssal boundary current, but much returns eastwards with the ACC flow. Furthermore, when the deep-reaching fronts of the ACC migrate to their more southerly climatological position, even into the northern Georgia Basin at the Falkland Gap as indicated in Fig. 9, Weddell Sea Deep Water may only escape the Georgia Basin toward the northeast. Thus, the southern region of the Argentine Basin, which extends to the east of the gap in the Falkland Ridge, is likely to receive a more direct and continuous inflow of the relatively colder waters from the Georgia Basin, enhanced perhaps by possible leakage through the multiple fractures in the Islas Orcadas Rise (Fig. 9).

The Subantarctic Front loops twice cyclonically across the SAVE line: first near 56°W, around stas. 174–181, and then more tightly near 30°W, around sta. 194 (Orsi et al., 1995; Tsuchiya, Talley & McCartney, 1994). This second (eastern) loop results in Weddell Sea Deep Water returning eastward to the north of the Falkland Plateau also being deflected to the northwest near 30°W. This latter cyclonic circulation in the southeastern Argentine Basin is clearly suggested by deep property distributions (Coles, McCartney, Olson & Smethie, 1996) and our AABW mean CFC-11 distribution in Fig. 7(a). It tends to further mix and recirculate Weddell Sea Deep Water within the abyssal layer of this basin before turning back to the southeast between the Islas Orcadas Rise and the Mid-Atlantic Ridge.

This circulation pattern may explain a puzzling observation in Fig. 11: that the highest bottom CFC concentrations (CFC-11 > 0.2 pmol kg^{-1}) are not found at the western boundary current but are banked on the western flank of the Mid-Atlantic Ridge, within a thin bottom layer with the densest ($\gamma^n > 28.31$ kg m^{-3}), coldest ($\theta < -0.25$°C), and freshest ($S < 34.66$) Weddell Sea Deep Water. These extreme near-bottom characteristics appear east of sta. 190, which is located just north of the gap in the Falkland Ridge, in a region where the deep density field clearly indicates the cyclonic loop of the Subantarctic Front around sta. 194. The latter is indicated by a narrow doming of isopycnals throughout the water column which, relative to the bottom, represents a clockwise geostrophic flow of Weddell Sea Deep Water and Circumpolar Deep Water between stas. 190–204 at depths greater than 3000 m. The opposite characteristics are found to the west of sta. 190: lower concentrations of CFC-11 (< 0.075 pmol kg^{-1}) are present in the deep waters found below 3000 m between stas. 186 and 190 in Fig. 11(b). All deep isopycnals show a trough between stas. 182–188 (Fig. 11(a)), indicating an anticlockwise geostrophic flow relative to the bottom. CFC-poor waters carried by the latter flow include some North Atlantic

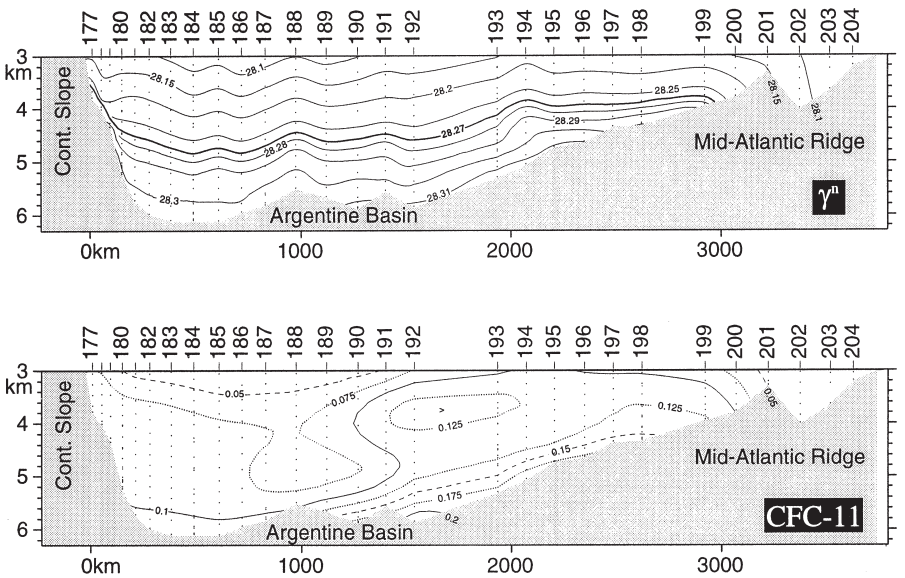

Fig. 11. Neutral density γ^n (kg m^{-3}) and CFC-11 (pmol kg^{-1}) along the SAVE section of 1988 extending zonally across the southern Argentine Basin near 47°S. See Fig. 9 for section location.

Deep Water ($\gamma^n < 28.15$ kg m^{-3}), recently incorporated into the ACC over the northwestern corner of the Argentine basin, as well as some Weddell Sea Deep Water and Circumpolar Deep Water returning southward from the western boundary current along the Subantarctic Front (stas. 181–182). At this southern location the North Atlantic Deep Water is so far from its source that it is characterized by a mid-depth CFC-minimum (CFC-11 $<$ 0.05 pmol kg^{-1}).

Direct lateral ventilation from the northern Georgia Basin to the southeastern Argentine Basin is also inferred in the ACCbw ($28.18 < \gamma^n < 28.27$ kg m^{-3}) at stas. 191–193. The isolated deep CFC-maximum (CFC-11 $>$ 0.125 pmol kg^{-1}) at 3400–4000 m is further evidence that remnants of well-ventilated Shelf Water mixtures exported at the Weddell–Scotia Confluence, like that seen at stas. 114–111 (near 1000–2000 m) in Fig. 10, are actually injected to the World Ocean: they manage to cross all three fronts of the ACC in the relatively short transit through the Scotia and Georgia basins.

4.3. Weddell Gyre

The most recently ventilated deep and bottom waters formed along the Antarctic margins of the Weddell–Enderby Basin are carried cyclonically along the outer rim of the Weddell Gyre, encircling and mixing with relatively older overlying interior waters—a pattern clearly depicted in Fig. 7(a) by the AABW with CFC-11 $>$ 0.2 pmol kg^{-1}. After moving along the northern limb of the Weddell Gyre, the relatively new Weddell Sea Bottom Water ($\gamma^n > 28.40$ kg m^{-3}) seen at the foot of the

America–Antarctic Ridge (stas 100–96 in Fig. 10(b)) is found at the AJAX (Fig. 12) section along the Greenwich Meridian. The water mass boundary separating the ACC and the Weddell Gyre regimes is located at sta. pair 79–80 (Orsi et al., 1995). At the northern limb of the gyre, at stas. 83–82, the well-ventilated characteristics of this bottom water are clear: CFC-11 > 0.2 pmol kg^{-1} and $H_2SiO_4 < 120$ μmol kg^{-1} for $\gamma^n > 28.40$ kg m^{-3}. But at the southern end of this section, banked against the Antarctic slope, the overlying Weddell Sea Deep Water ($28.34 < \gamma^n < 28.40$ kg m^{-3}) shows even higher CFC concentrations (CFC-11 > 0.25 pmol kg^{-1} at sta. 93) than the Weddell Sea Bottom Water at the northern limb. This southern maximum contains the best ventilated (minimum pCFC-11 apparent age) water below 1000 m along this section. It has been repeatedly observed at the base of the continental slope after the AJAX section of 1984, e.g. south of Maud Rise during the winter German Antarctic Expedition (ANT V/3) of 1987 (Weiss, 1987; Schnack-Schiel, 1987) and more recently near 17°W during the winter WOCE A23 line of 1995 (Van Scoy, Locarnini, Watson, Meredith, Heywood et al., 1999). Although this signal coincides with a near bottom silica minimum ($H_2SiO_4 < 125$ μmol kg^{-1}), no corresponding signal is evident in the thermohaline fields. Nevertheless, at this longitude westward spread of a new type of bottom water is inferred (Fig. 7(a)) along the lower portion of the continental slope, most likely originating from a source near the Amery Ice Shelf (Jacobs & Georgi, 1977).

At the northern limb of the gyre, lateral ventilation by eastward flow of Weddell–Scotia Confluence water remnants (Whitworth & Nowlin, 1987) is evident at stas 82–80 at all depths above 3000 m ($\gamma^n < 28.34$ kg m^{-3}), where CFC concentrations are consistently high (CFC-11 > 0.125 mol kg^{-1}) and uniform vertically. The cyclonic circulation along the outer part of the gyre brings some of these well-ventilated near-surface waters to the southern limb, contributing to the subsurface (400–600 m) CFC-maximum (> 0.25 pmol kg^{-1}) at stas 91–90. Offshore export of high-CFC (> 1 pmol kg^{-1}) surface waters carried to the west within the Antarctic Slope Current (Whitworth et al., 1998) could reinforce the last northern near-surface signal: isopycnals dome in the upper 1000 m between stas 94–90, reflecting a small clockwise cell that would facilitate the export of coastal surface waters to more northern latitudes. In Fig. 12(b) relatively high CFC concentrations (CFC-11 > 0.05 pmol kg^{-1}) extend both northward into the gyre's southwestward-flowing limb (stas 89–87) and downward to 1000 m, i.e. well into the source waters imported from the ACC at the gyre's eastern limb. Thus, Circumpolar Deep Water imported from the ACC is ventilated laterally from the north as well as from the south as it progresses southwestward along the gyre's southern limb (stas 84–92).

In the Weddell Gyre, ACCbw with $28.23 < \gamma^n < 28.27$ kg m^{-3} is indicated by the CFC-minimum (CFC-11 < 0.05 pmol kg^{-1}) sloping downward from about 1000 m at the dome's axis (sta. 85) to near 1400 m at sta. 93. It lies just below the oxygen minimum that characterizes Central Intermediate Water (Whitworth & Nowlin, 1987) trapped and recirculating inside the gyre's center, so it is not surprising that this CFC-poor water has the oldest apparent pCFC-11 ages along this section; i.e. it constitutes the least ventilated water in Fig. 12(b). The intermediate silica maximum ($H_2SiO_4 > 128$ μmol kg^{-1}) observed between stas. 88 and 83 is also expected, since

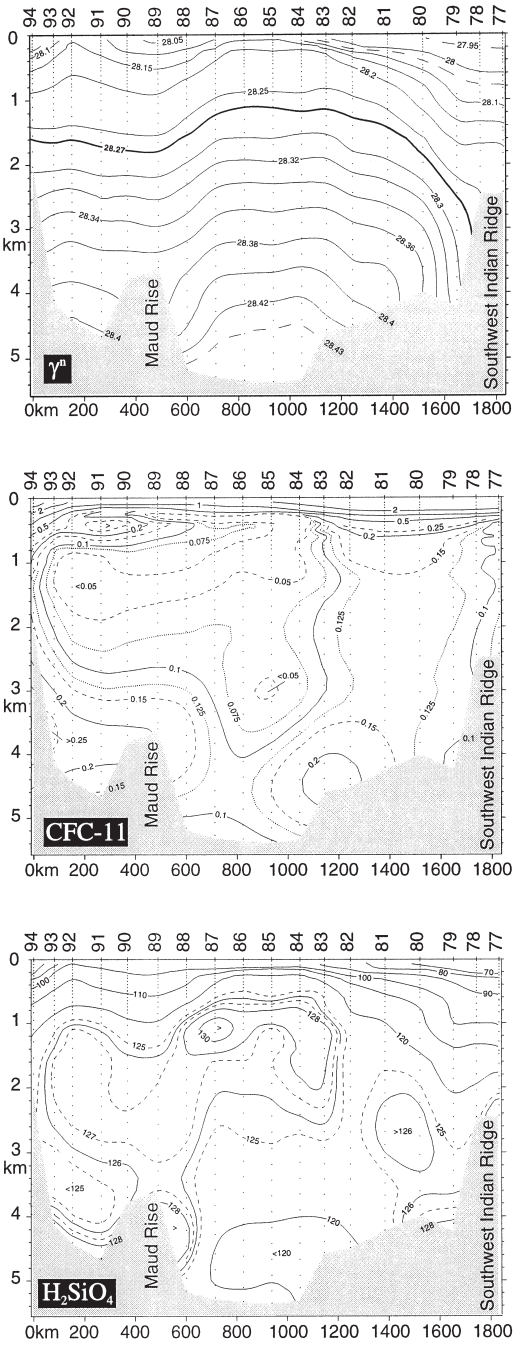

Fig. 12. Neutral density γ^n (kg m^{-3}), CFC-11 (pmol kg^{-1}), and silica H_2SiO_4 (μmol kg^{-1}) along the AJAX section of 1984 extending meridionally across the Weddell Gyre near the Greenwhich Meridian. See Fig. 9 for section location.

ACCbw in the Weddell Gyre is ultimately derived from Drake Passage, via eastward flows along the southern fringes of the ACC to near 20°–30°E. This same density layer ($28.23 < \gamma^n < 28.27$ kg m^{-3}) already shows $H_2SiO_4 > 135$ μmol kg^{-1} at the bottom of the Southeast Pacific Basin (Sievers & Nowlin, 1984). Attenuation of the high-silica signal in the ACCbw takes place during its long eastward transit through mixing with less enriched waters both above (North Atlantic Deep Water) and below (Weddell Sea Deep Water); thus, relatively lower silica concentrations ($H_2SiO_4 =$ 126 μmol kg^{-1}) are already observed at the bottom of stas 77, near the poleward end of the ACC (Fig. 12(c)) than at Drake Passage. Whitworth and Nowlin (1987) suggested that the silica increase observed between these ACC stations and the interior of the gyre could be produced by resuspension of bottom sediments off the flanks of the Southwest Indian Ridge and Conrad Rise, as Lower Circumpolar Deep Water leaves the ACC and enters the gyre around its northeastern end (54°S, 30°E). Carmack (1973) postulates that further in-situ silica gain results from recirculation inside the gyre just underneath the layer where particulate dissolution and nutrient regeneration take place (i.e. at the oxygen minimum and nutrient maximum cores).

Downward tilt of isopycnals over the eastern limb of the Weddell Gyre connects mid-depth waters of the Weddell Sea ($\gamma^n > 28.27$ kg m^{-3}) with near-bottom waters of the Enderby Basin, where dense Weddell Sea waters mix with the local silica-rich bottom waters ($H_2SiO_4 > 140$ μmol kg^{-1}). Consequently, deep and bottom waters entering the gyre from the east at stas. 89 and 88 reflect this prominent influence from the Enderby Basin in the relatively high silica values seen at all depths below 1500 m (Fig. 12(c)). The strongest signal is found for $28.38 < \gamma^n < 28.42$ kg m^{-3} at the bottom of stas. 94–88. Silica-poor bottom water types produced more recently along the western Weddell Sea ($\gamma^n > 28.40$ kg m^{-3}) and the Amery Ice Shelf ($28.34 < \gamma^n < 28.39$ kg m^{-3}) erode this high-silica signal imported from the Enderby Basin once it has entered and been recirculated within the gyre. This signal may completely disappear farther downstream over the southwestern Weddell Sea, where the newly-formed Weddell Sea Bottom Water is found at the slope containing much less silica than observed in water at the Greenwich Meridian.

The upper, less dense portion of Weddell Sea Deep Water ($28.27 < \gamma^n < 28.34$ kg m^{-3}) displays an almost continuous silica-rich band at mid depths (near $\sigma_2 = 37.18$ kg m^{-3}; Whitworth & Nowlin, 1987) with $H_2SiO_4 > 127$ μmol kg^{-1}. As already described for the overlying Lower Circumpolar Deep Water layer, lateral mixing with the more ventilated peripheral waters of the gyre is the dominant process eroding this core at stas. 94, 90, and 82.

4.4. ACC Bottom Water ventilation by Antarctic Bottom Water upwelling

A potential mechanism contributing to the high CFC signal observed at the bottom of the ACC, i.e. on $\gamma^n = 28.27$ kg m^{-3}, where rapid upwelling is expected, is intensified vertical mixing with well-ventilated bottom waters below. Patterson and Sievers (1980) suggested that increased vertical mixing within bottom layers over shallow bathymetry could explain the characteristic homogeneity observed in the water mass stratification of the Weddell–Scotia Confluence region. They proposed that the inter-

action of currents with the South Scotia Ridge induces relatively strong vertical mixing and stirring at the bottom of the water column. An example of this topographic interaction is seen on the vertical distribution of CFC-11 from the AJAX stations that cross the Weddell–Scotia Confluence near 50°W (see Fig. 2 of Whitworth et al., 1994). There the transition between ACCbw and AABW is represented by the deep layer with potential temperatures between -0.2°C and -0.4°C. Note that the most extreme AABW characteristics within that deep transitional layer (CFC-11 > 0.4 pmol kg^{-1}, and $S < 34.66$) are found at sta. 126 and 127, located directly over the sill of the South Scotia Ridge. In contrast to the signal in the intermediate waters (400–1300 m) of the Weddell–Scotia Confluence ($\theta > -0.2$°C at sta. 119–127), the deeper high-CFC signal clearly is gained from the Weddell Sea Deep and Bottom Waters below (CFC-11 > 0.6 pmol kg^{-1}) pressed against the southern flank of the ridge. Obviously, lateral and upward ventilation at deep levels of the ACC are both strongest in the southern Scotia Sea, a point already made in Section 2, and through a regional study of the deep thermohaline structure (Locarnini et al., 1993). Next we will show evidence of regions with favorable conditions for vertical mixing along the sections in the southern South Atlantic discussed above.

Time-dependent tracers offer a good opportunity to investigate whether there are any preferred sites with enhanced upward mixing of AABW and densest Circumpolar Deep Water of the ACC. Ideally, where there is active water mass conversion by upward entrainment of AABW into the ACCbw one expects to find CFC concentrations on $\gamma^n = 28.27$ kg m^{-3} that are closer to those of the better ventilated waters found immediately underneath. Thus deep isopycnal surfaces may indicate areas of enhanced vertical mixing where denser water parcels have had a relatively shorter time to mix laterally with the surrounding waters before their upward entrainment. While temperature and salinity distributions ought to reveal these features, they are ambiguous because they also determine the density of the water parcel, whereas CFC concentrations are completely independent of seawater density.

Upward mixing of relatively young Weddell Sea Deep Water is vigorous over the rough topography of the eastern Scotia Sea. As shown in the previous example at 50°W, this mechanism is also implied from the observed CFC-11 concentrations on $\gamma^n = 28.27$ kg m^{-3} (Fig. 13(a)), which corresponds to the AJAX section across the South Sandwich system (Fig. 10). The degree of vertical ventilation observed in some places at the bottom of the Circumpolar Deep Water depends, in part, on how close $\gamma^n = 28.27$ kg m^{-3} lies both to the underlying well-ventilated Weddell Sea Bottom Water as well as to the CFC-poor water above. At stas 116–115, $\gamma^n = 28.27$ kg m^{-3} lies above CFC-rich Weddell Sea Deep Water (CFC-11 > 0.35 pmol kg^{-1}), where the water is expected to upwell rapidly as a result of the topographic interaction with the flow. These conditions may explain why the concentrations on that isopycnal are the highest at sta. 116–114 (CFC-11 about 0.3 pmol kg^{-1}). Between stas. 106–101, $\gamma^n = 28.27$ kg m^{-3} lies farther not only from an 'older' Weddell Sea Deep Water (CFC-11 > 0.25 pmol kg^{-1}) but also closer to overlying CFC-poor waters (CFC-11 < 0.2 pmol kg^{-1}), all of which act to reduce the local concentrations significantly to about 0.2 pmol kg^{-1}.

Entrainment of CFC-rich Weddell Sea Deep Water up into the bottom of the ACC

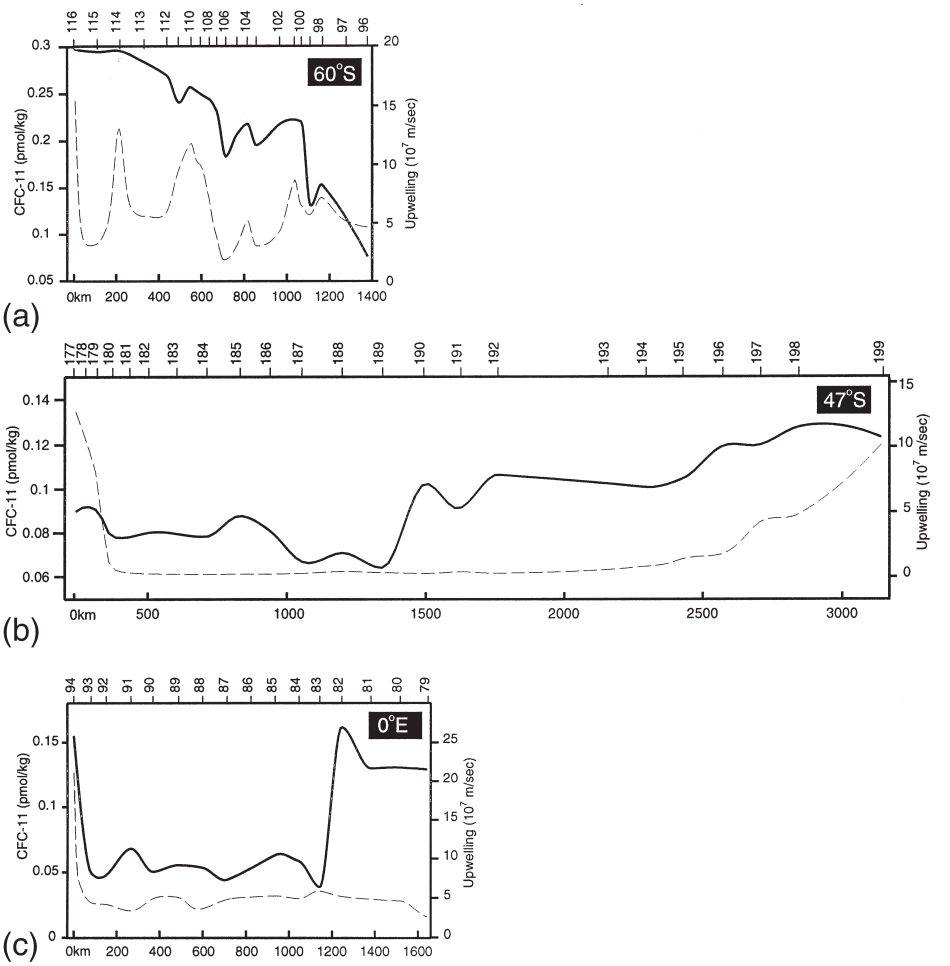

Fig. 13. Measured CFC-11 (pmol kg^{-1}) distributions at $\gamma^n = 28.27$ kg m^{-3} along (a) the AJAX section across the South Sandwich system, (b) the SAVE section across the southern Argentine Basin, and (c) the AJAX section across the Weddell Gyre. See Fig. 9 for station locations. Dashed lines are the corresponding modeled upwelling speed (m s^{-1}) discussed in Section 5.2.

is also favored over the southeastern Argentine Basin. Along the SAVE section near 46°S (Fig. 11), mixing across this density horizon ($\gamma^n = 28.27$ kg m^{-3}) appears to be considerably higher to the east of sta. 195 (Fig. 13(b)), i.e. along the sluggish (broad) southeastward return flow of relatively cold Weddell Sea Deep Water imported from the Georgia Basin. The more ventilated AABW layer thins out dramatically there, along the weak incline of the Mid-Atlantic Ridge, and local topographic and turbulent mixing must increase the CFC-11 concentrations (> 0.12 pmol kg^{-1}) on $\gamma^n = 28.27$ kg m^{-3}.

For the AJAX section (Fig. 12) at the Greenwich Meridian, Fig. 13(c) suggests

considerable vertical mixing is occurring near the Antarctic slope regime (sta. 94). There $\gamma^n = 28.27\ kg\ m^{-3}$ lies close to recently-formed bottom water (3500 m) advected from its source near the Amery Basin along the lower portion of the slope (Fig. 7(a)). Thus relatively high concentrations (CFC-11 > 0.15 pmol kg^{-1}) are seen on $\gamma^n = 28.27\ kg\ m^{-3}$ at sta. 94, which are about three times larger than within the interior of the gyre at the same density surface. CFC-11 on $\gamma^n = 28.27\ kg\ m^{-3}$ also shows evidence of significant ventilation to the north of sta. 83 (CFC-11 > 0.125 pmol kg^{-1}). All these stations, in particular sta. 82, reflect the influence of both lateral and vertical ventilation of the whole water column that has taken place farther upstream within the Weddell–Scotia Confluence. This relatively well-ventilated and homogenized layer found at intermediate to mid-depths (1000–3500 m) is receiving the local high-CFC signal from the upwelling of newly-formed Weddell Sea Bottom Water spreading eastward at relatively deeper levels (near 4500 m), along the southern rise of the America–Antarctic and Southwest Indian ridges.

5. Antarctic Bottom Water production

Previous estimates of the rates at which new bottom waters are formed around Antarctica resulted from various indirect approaches, or a combination of them; but they all strongly depended on the spatial scales analyzed and on the assumed mixing recipes. One approach relied on property distributions and computed volume transports at the western boundary current of the Weddell Gyre, usually partitioned into newly-formed bottom water sinking toward the bottom of the slope and older, less-dense deep water recirculating within the interior (Carmack & Foster, 1975). Another method was based on rough estimates of the residence time of near-freezing Shelf Water (3 to 7 years, see Gill, 1973) over the Antarctic shelves before they are exported and can contribute to bottom water formation processes. Similar assumptions were made in production rate estimates based on modeled Shelf Water budgets including a variety of geochemical tracers (Mensch et al., 1997). Most of these methods arguably assumed some entrainment rate of lighter ambient waters into the sinking shelf water mixtures, before they actually manage to reach the abyssal depths offshore. A few estimates of bottom water production in Antarctica are listed in Table 3; again, perhaps the most critical point in most of these estimates is, ultimately, their strong dependence on mixing recipes leading to bottom water formation.

In this study, the total volume of newly-formed bottom water sinking across the 2500-m isobath of the Antarctic slope, and thus filling the oceanic bottom layer shown in Fig. 7, represents the total production rate of AABW ($\gamma^n > 28.27\ kg\ m^{-3}$). Near-boundary convection also replenishes the relatively less dense waters above AABW (see Fig. 5), but those volumes are not included here. In the following estimates of the total production rate of AABW we assume that: (a) newly-formed bottom waters sinking to great depths at the continental margins undergo most of the entrainment of environmental waters upon reaching the 2500-m isobath; (b) the rate is equal to the net offshore transport across the continental 2500-m isobath beneath $\gamma^n = 28.27\ kg\ m^{-3}$; (c) all AABW must upwell out of the bottom layer into the ACCbw layer above.

Table 3
Estimates of Antarctic Bottom Water production rates

From	Water mass	Production rate (10^6 m^3 s^{-1})
DWBC Transport		
Carmack and Foster (1975)	WSBW ($\theta = -1.2$°C $-$ 1.4°C)	2–5
Foster and Carmack (1976)	WSBW ($\theta = -1.3$°C)	3.6
Foldvik et al. (1985)	WSBW ($\theta = -0.8$°C)	2
Gordon et al. (1993)	WSBW ($\theta < -0.8$°C)	3
Fahrbach et al. (1995)	WSBW ($\theta < -0.7$°C)	2.2
Muench and Gordon (1995)	WSBW ($\theta < -0.8$°C)	2.5–3
Speer and Forbes (1994)	Indian AABW ($\theta < 0$°C)	1
Gordon (1998)	WSBW ($\theta = -1.1$°C, $\theta < -0.7$°C)	3–4
Shelf Water budgets		
Gill (1973)	AABW ($\theta = -0.6$°C)	10–15
Gordon (1974)	RSBW ($\theta = -0.6$°C)	5
Carmack (1977)	AABW ($\theta = -0.6$°C, $\theta < 0$°C)	5–10
Jacobs et al. (1985)	AABW ($\theta = -0.8$°C)	13
Natural and anthropogenic tracer budgets		
Weiss et al. (1979)	WSBW ($\theta < -0.9$°C)	3–5
Weppernig et al. (1996)	WSBW ($\theta < -0.7$°C)	5
Mensch et al. (1997)	WSBW ($\theta < -1$°C)	3.5

Next, an independent, tightly constrained estimate of the total production of AABW around Antarctica is presented, for the first time, taking advantage of the CFC-11 distribution shown in Fig. 7(a).

5.1. Chlorofluorocarbon budget

Shelf waters around Antarctica carry a relatively high level of dissolved CFCs. At the Antarctic slope, as shelf waters sink and mix with ambient waters to form new bottom water types, they inject CFCs into the oceanic AABW layer. Thus, the total inventory of CFCs in the AABW layer reflects the accumulation of CFCs carried by these newly-formed source waters, minus the export of CFC-bearing AABW out of the layer. In deriving a CFC budget we will consider the total transport of newly-formed AABW varieties sinking across the slope's 2500-m isobath (T_I) as being the effective 'oceanic source' of CFC for the offshore bottom layer beneath $\gamma^n = 28.27$ kg m^{-3}, and equal to the global production rate of AABW.

The concentration of CFC-11 in the atmosphere has increased as a function of time. Thus the equilibrium concentration of CFC-11 in new AABW types also varies with time; it is proportional not only to the atmospheric CFC-11 concentration but also to the solubility coefficient for CFC-11 in seawater, which is a simple function of temperature and salinity (Warner & Weiss, 1988). Because very small ranges of temperature and salinity (1°C and 0.2, see Fig. 3(b)) are observed in newly-formed

AABW types, the solubility coefficient (K) for CFC-11 will be treated as a constant below. Thus at any time the concentration of CFC-11 in newly formed AABW is given by:

$$\text{CFC-11}_{AABW} = \text{CFC-11}_{atm} \cdot K \cdot \text{SAT}_{CFC\text{-}11}$$

where $\text{CFC-11}_{\text{atm}}$ is the concentration (mole fraction) of CFC-11 in the atmosphere, and $\text{SAT}_{\text{CFC-11}}$ is saturation level of CFC-11 in new AABW, i.e. the ratio of observed to equilibrium concentrations of dissolved CFC-11. A number of measurements of $\text{SAT}_{\text{CFC-11}}$ have been made in recently formed AABW at depths near the continental rise (Table 4). In the derivation below, we assume that the $\text{SAT}_{\text{CFC-11}}$ in new bottom water types has remained constant over the time history of atmospheric input.

The cumulative oceanic input of CFC-11 into the oceanic bottom layer, by means of AABW production (T_{I}) from the initial release of CFC-11 into the atmosphere to the present time, is equal to the current CFC-11 content (inventory) minus any cumulative output (L) of CFC-11 out of the oceanic bottom layer and into the ACCbw above:

$$\int_{V_{\text{AABW}}} \text{CFC-11}_{AABW} \cdot \mathrm{d}v = T_{\text{I}} \cdot K \cdot \text{SAT}_{CFC\text{-}11} \cdot \int_{t_0}^{t} \text{CFC-11}_{atm} \cdot \mathrm{d}t + L$$

Since the relative CFC-11 in new AABW types is about an order of magnitude higher than the average CFC-11 for the oceanic AABW layer (Tables 2 and 4), we assume that the loss term (L) is only a small fraction of the oceanic source term. At this point we neglect L, but an estimate of its magnitude is provided at the end of this section.

The Atlantic sector was sampled during the eighties (1984 to 1990), whereas the

Table 4
Characteristics of known Antarctic Bottom Water types and their Lower Circumpolar Deep Water sources

	Cruise/Sta.	Depth (m)	γ^n (kg m^{-3})	θ (°C)	S	CFC-11 (pmol kg^{-1})	$\text{SAT}_{\text{CFC-11}}$ (%)
35°W—1987							
WSBW	ANTV4/775	2141	28.474	− 1.236	34.610	2.312	36.47
LCDW		1200	28.21	0.314	34.682	0.181	3.16
140°E—1991							
Adélie BW	SR3/27	3687	28.376	− 0.796	34.649	2.573	35.11
LCDW		1200	28.15	0.924	34.721	0.094	1.44
170°E—1992							
RSBW (high S)	PS4/774	2700	28.470	− 0.767	34.725	2.524	35.06
RSBW (low S)	PS4/770	3100	28.32	− 0.133	34.692	0.925	13.36
LCDW	PS4/770	1400	28.19	0.618	34.706	0.029	0.44

Indian–Pacific sector was sampled more recently (1991 to 1996). To minimize the temporal bias in the measurements, different upper limits in the time integration of the atmospheric CFC-11 were set. Thus, 1987 and 1993 were used for the Atlantic and Indian–Pacific sectors, respectively (Table 5). A reconstructed atmospheric history of CFC-11 concentration for the Southern Hemisphere was used in this calculation (Walker, Salmeh & Weiss 1995, personal communication).

Available measurements of CFC-11 only allow us to determine the characteristic $SAT_{CFC\text{-}11}$ observed at the 2500-m isobath for locations close to the four well-known sources of bottom water types (Table 4); namely the Weddell Sea Bottom Water, Adélie Land Bottom Water, and both high-salinity and low-salinity Ross Sea Bottom Water. Inclusion of other significant sources of AABW types with potentially different saturation levels, e.g. those near the Larsen, Amery, West, and Shackleton Ice shelves, might well modify our CFC-11 inventory (volume integral). However, saturation levels for three of the four sampled contributors show little variability. Moreover, if the low-salinity Ross Sea Bottom Water had been sampled closer to its source region in the eastern shelf of the Ross Sea (Trumbore, Jacobs & Smethie, 1991) it seems likely that the $SAT_{CFC\text{-}11}$ for this type would also be close to the mean value (35%) observed for the other types. If this observation holds true for all of the unsampled sources of bottom water types, then their inclusion in our oceanic budget would not affect significantly the final global production rate of AABW estimated here, where we assume a spatially uniform $SAT_{CFC\text{-}11}$ of 35%.

In contrast to the roughly similar CFC-11 and saturation levels in all new AABW types, considerable variability is observed in the source Lower Circumpolar Deep Water near the AABW production sites (Table 4). The Indian sta. 27 (SR3, 140°E) is located at the southernmost fringes of the ACC whereas all other stations are located at the southwestern edges of the subpolar cyclones, where only older remnants of recirculating Lower Circumpolar Deep Water from the ACC are found. Lower Circumpolar Deep Water in the interior of the Ross Gyre is about an order of magnitude more under-saturated than the relatively colder and less saline Lower Circumpolar Deep Water in the Weddell Gyre. This fact, together with similar evidence from the apparent CFC-11 ages, indicates that the ACCbw in the Weddell–Enderby Basin must be ventilated more rapidly than in the Southeast Pacific Basin because of the larger production of AABW in the Atlantic sector.

Table 5
Production rates of newly-formed Antarctic Bottom Water sinking downslope

	Oceanic CFC-11 budget		
	Content (10^6 moles)	Oceanic input/T_I (moles s m^{-3})	Production (T_I) (10^6 m^3 s^{-1})
Atlantic	6.182 (norm. 1987)	1.266 (up to 1987)	4.9 (60%)
Indian + Pacific	4.812 (norm. 1993)	1.514 (up to 1993)	3.2 (40%)
Total			8.1

During the mixing taking place near the shelf break to form new AABW, the CFC contribution from the Lower Circumpolar Deep Water is small (insignificant if we assume that Lower Circumpolar Deep Water is CFC-free), whereas the contribution from the Shelf Water to AABW is clearly dominant. It is the relative proportion of Lower Circumpolar Deep Water volume that is being mixed with Shelf Water which determines the final CFC content of the end product. For example if the mixing of CFC-poor ($SAT_{CFC\text{-}11} = 0.02$) Lower Circumpolar Deep Water with more ventilated Shelf Water ($SAT_{CFC\text{-}11} = 0.6$) rendered the observed $SAT_{CFC\text{-}11}$ of 35% in all AABW types, then one would expect a nearly constant entrainment rate of Lower Circumpolar Deep Water that roughly doubles the volume of the original Shelf Water component.

A total production rate of 8.1 Sv of AABW is indicated by this oceanic CFC-11 budget (Table 5). The Atlantic sources contribute 60% of this total, and the remaining sources in the Indian and Pacific sectors the other 40%. This estimated 8.1 Sv of newly-formed bottom waters is a minimum, since we have not taken into account the small loss of CFC-bearing AABW that has been lost from the bottom layer during most recent years by upwelling through $\gamma^n = 28.27\ kg\ m^{-3}$. At present the outflowing waters at the top isopycnal have a much lower CFC-11 content (see Fig. 13) than the inflowing 'source' AABW types (Table 4), thus the net loss of CFC-11 is likely to be small.

A rough estimate of the magnitude of the time-dependant loss (L) of CFC out of the AABW layer is derived by considering two extreme mixing models: a bottom layer with no-mixing and a well-mixed bottom layer. In the former scenario the CFC-signal is injected at the bottom of the layer, after which it moves upward through a mean layer thickness of about 1470 m with an average speed of $2.5 \times 10^{-7}\ m\ s^{-1}$ (calculated using 8.1 Sv as the total production rate of AABW and the total areal extent of the top isopycnal). It would take about 187 years for the CFC-signal to reach the top isopycnal in the no-mixing model, and so would make no contribution to L over the 1930–1987 (–1993) integration period in the Atlantic (Indian and Pacific) sector. In contrast, if the bottom CFC-signal is instantaneously mixed within the AABW layer, i.e. a well-mixed model, at any given time, the exported water at the top isopycnal would contain the layer-average concentration. Assuming uniform increase for the bottom layer's mean CFC concentration, i.e. from $0\ pmol\ kg^{-1}$ in 1930 to $0.22\ pmol\ kg^{-1}$ in 1990, and the same average upward speed as before ($2.5 \times 10^{-7}\ m\ s^{-1}$), a total of 1.8×10^6 moles of CFC-11 would have escaped across the top isopycnal between 1930 and 1990. Adding this loss term (L) to the CFC-11 content in Table 5 yields an additional 1.3 Sv to the total production rate of AABW. It is encouraging that the estimated global formation rate of AABW based on our oceanic CFC-budget of 8.1–9.4 Sv, falls nicely within the 5–10 Sv range derived by Carmack (1977) from his global Shelf Water budget. Next, we examine the corresponding oceanic mass-budget for the AABW layer.

5.2. Mass budget

Vertical outflow of AABW is distributed over the vast surface area between the 2500-m isobath and the more northern locations where $\gamma^n = 28.27\ kg\ m^{-3}$ intersects

the bottom topography. Thus, the total volume of AABW (V) is computed as the surface integral over the $\gamma^n = 28.27\ \mathrm{kg\ m^{-3}}$ area (A) of its height above the ocean floor (H), i.e.

$$V = \int\int H\, dA$$

Similarly, the total production rate of AABW is

$$T = \int\int W\, dA$$

One can either assume a uniform (constant) upwelling speed throughout the top of the layer, or a spatially varying speed.

Numerous estimates of deep upwelling speeds have been reported in the literature (Table 6), yielding magnitudes varying by about three orders, depending on the spatial scale analyzed. For instance, turbulent upwelling rates near deep narrow passages can reach values well over $100 \times 10^{-7}\ \mathrm{m\ s^{-1}}$, whereas microstructure measurements in the vast interior regions of the ocean imply vertical speeds as low as $0.1 \times 10^{-7}\ \mathrm{m\ s^{-1}}$. If a constant upwelling velocity is applied at the top of the AABW layer using values listed in Table 6, the extreme values yield totally unrealistic results when compared with the observed meridional circulation of the Southern Ocean. While a vigorous turbulent upwelling rate would require more than 300 Sv of AABW to be formed around Antarctica, an almost quiescent interior upwelling would only demand about 0.3 Sv. Most basin-wide estimates of deep upwelling require, to balance the deep heat budget in the Southern Hemisphere, speeds that range typically

Table 6
Various estimates of deep upwelling rates

Work	Region	Upward speed ($10^{-7}\ \mathrm{m\ s^{-1}}$)	Method or scale
Kunze and Sanford (1996)	Sargasso Sea	0.1	Microstructure
Toole et al. (1994)	NE Atlantic and Pacific	0.1	Microstructure
Stommel and Arons (1960a, 1960b)	World Ocean	0.5	Global
Warren (1981b)	Atlantic Ocean	0.8	Trans-Ocean
	Pacific Ocean	1.3	Trans-Ocean
Munk (1966)	Pacific Ocean	1.4	Data, models
Stommel (1958)	World Ocean	1.5	Global
Johnson (1990)	Equatorial Pacific	1.8	Trans-Ocean
Speer and Zenk (1993)	Brazil Basin	2	Basin
Robbins and Bryden (1994)	North Pacific	2–2.8	Trans-Ocean
Warren and Speer (1991)	Angola Basin	3.1	Basin
Warren (1981b)	Indian Ocean	4	Trans-Ocean
Robbins and Toole (1997)	Indian Ocean	4.5	Trans-Ocean
Whitehead and Worthington (1982)	Western North Atlantic	6.5	Basin
Toole and Warren (1993)	Indian Ocean	6.9	Trans-Ocean
Hogg et al. (1982)	Vemma Fracture Zone	10	Sub-basin
Johnson (1990)	Somali Basin	12	Basin
Roemmich et al. (1996)	Samoan Passage	20–1000	Sub-basin
Polzin et al. (1996)	Romanche Fracture Zone	100–1000	Microstructure

between 1 and 7×10^{-7} m s^{-1}. Uniform upwelling at the top isopycnal with speeds similar to those inferred from deep ocean-scale heat budgets yield production rates of AABW that are in remarkable agreement with previous estimates resulting from global shelf water budgets. An average deep upwelling speed of 3×10^{-7} m s^{-1}, i.e. the mean speed inferred in the South Atlantic, Indian, and Pacific Oceans (Warren, 1981b; Toole & Warren, 1993), yields 10 Sv of AABW production: the upper limit of Carmack's (1977) estimate. Our previous CFC-budget also points to a similar upwelling rate of 2.5×10^{-7} m s^{-1} at the top isopycnal.

Despite this consistency, it seems more likely that there are small areas of the abyssal ocean where vertical mixing and upwelling are dramatically intensified above a rather lower background than for the distribution to be uniform. Such areas will include the regions where swift abyssal boundary currents are forced to pass through narrow gaps in the bottom ridges, where turbulent hydraulic interaction enhances vertical mixing within the bottom layer by a couple of orders of magnitude. This mechanism is implied just downstream of the Samoan (Roemmich, Hautala & Rudnick, 1996) and Romanche (Polzin, Speer, Toole & Schmitt, 1996) passages. Flow over prominent topographic features also imposes stronger upwelling and vertical stirring on relatively shallow water columns (Gill, 1977). At certain locations the top of AABW, $\gamma^n = 28.27$ kg m^{-3}, also shoals enough to be directly influenced by atmospheric forcing. This is the case along the vast elongated doming of the central Weddell Gyre, where wind-induced upwelling adds to the background buoyancy forcing represented by the sinking of newly-formed shelf water mixtures across the shelf break.

Next we present an ad-hoc parametrization of the upward entrainment rate of AABW into the less dense ACCbw above based on the depth of $\gamma^n = 28.27$ kg m^{-3} (Z), the water depth (D), and the bottom layer thickness (H). We attempt to incorporate the wind, bottom, and turbulent influences on the upwelling rate (W) while quantifying its spatial distribution at the top of the AABW (Fig. 14). Here,

$$W = w_w + w_b + w_t = w_1 + w_2 + w_2 \cdot w_3$$

where

$$w_1 = k_1 \cdot e^{-a_1 x_1} \text{ and } w_{2,3} = k_{2,3} \cdot e^{-(a_{2,3} \cdot x_{2,3})^2}$$

with

$$\begin{cases} k_1 = 15 \times 10^{-7}, \; a_1 = \dfrac{1}{1000 \text{ m}}, \; x_1 = Z \\ k_2 = 5 \times 10^{-7}, \quad a_2 = \dfrac{1}{2000 \text{ m}}, \; x_2 = D - 2000 \text{ m} \\ k_3 = 5 \times 10^{-7}, \quad a_3 = \dfrac{1}{500 \text{ m}}, \quad x_3 = H \end{cases}$$

The wind-driven upwelling component (w_w), represented here by an exponential of the isopycnal depth, is scaled by the entrainment rate at the base of the mixed layer

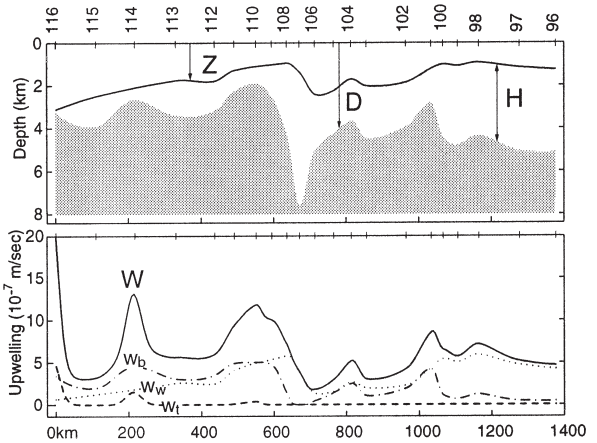

Fig. 14. Modeled upwelling speed (m s^{-1}) at $\gamma^n = 28.27$ kg m^{-3} along the AJAX section of 1984 extending southeastward across the South Sandwich system. *D* and *Z* indicate the bottom relief and depth of $\gamma^n = 28.27$ kg m^{-3}, whereas *H* represents the thickness of the bottom layer; w_w, w_b, and w_t are the modeled wind, bottom, and turbulent components of upwelling. See Fig. 9 for station locations.

reported by Gordon and Huber (1990) in the central Weddell Gyre (14.3×10^{-7} m s^{-1} at 135 m) assuming a length-scale of 1 km. A Gaussian function of the bottom topography represents the bottom component (w_b). This contribution is maximum at levels of roughly the shallowest topographic features cleared by $\gamma^n = 28.27$ kg m^{-3} ($D = 2000$ m), where above-average upwelling speeds ($w_b > 5 \times 10^{-7}$ m s^{-1}) are expected; its influence is set to diminish to typical interior values ($w_b < 0.5 \times 10^{-7}$ m s^{-1}) over the deeper interior ($D > 5000$ m). To reproduce the non-linear turbulent component (w_t) expected within thin bottom layers found over rough topography and at deep narrow gaps in the bottom ridges, the bottom component is multiplied by another Gaussian function of the layer thickness. Therefore the turbulent influence is restricted to deep bottom layers with a 500-m vertical length-scale, as suggested by Kunze and Sanford (1996), and peaks with relatively high speeds ($w_t = 25 \times 10^{-7}$ m s^{-1}) but still much lower than the values reported by Roemmich et al. (1996) and Polzin et al. (1996). This conservative approach is appropriate for the coarse resolution of our grid spacing of roughly 110 km. Since the spatial distribution of deep vertical mixing in the ocean is poorly constrained, there are many ways to model it, some of which would yield the same total transport across $\gamma^n = 28.27$ kg m^{-3}. The ad-hoc formulation described above is not meant to improve any estimate of the total production rate of AABW, but rather to suggest where in the Southern Ocean the AABW might mix upward and so ventilate the ACCbw layer more vigorously. The resulting distribution of upwelling at the top of the AABW layer is consonant to the observed CFC distribution on that isopycnal.

An example of the resulting upwelling distribution is given (Fig. 14) along the AJAX line (see Figs. 9 and 10) extending across the South Sandwich Trench. South of sta. 100, because both the water depth (*D*) and layer thickness (*H*) are relatively

large, the wind-component (w_w) is practically the only contributor to W, as it is over the Trench (sta. 108–106). At places where the bottom shoals, like near sta. 101, 104, and 110, the bottom (w_b) and wind components (w_w) are about the same. At sta. 110, which is located at the top of the South Sandwich Island Arc, W starts to include some small turbulent contribution (w_t) since there the layer's thickness is less than 800 m. North of sta. 113 $\gamma^n = 28.27$ kg m^{-3} lies below 2000 m, so w_w is no longer a major contributor, but at the same time the layer thickness decreases dramatically over the shallowest bottom topography.

At sta. 116 and 114 the AABW layer thins out to the point where w_t dominates the local upwelling, confirming that turbulent upwelling rates are expected in the southern Scotia Sea (Patterson & Sievers, 1980). On the average the upwelling rates along this section are above the estimates resulting from basin-scale budgets, as is reasonable for a rather small region with such a complex bottom topography like this one. Similar conditions are to be expected at several other places in the Southern Ocean.

Preferred sites for rapid vertical entrainment of AABW are clearly indicated in the spatial distribution of upwelling at $\gamma^n = 28.27$ kg m^{-3} (Fig. 15) from the ad-hoc approach discussed above. Areas where $W > 5 \times 10^{-7}$ m s^{-1} are in general agreement with our interpretation of tracer distributions are: (1) where there is relatively intense upwelling along the rise of the Antarctic continental slope, and vertical mixing is enhanced in thin benthic layers by bottom intensified currents carrying the newest bottom waters; (2) over the most prominent topographic features cleared by this isopycnal, like the South Scotia Ridge, South Sandwich Arc, and Maud Rise; (3) over both interbasin sills at the Princess Elizabeth and Balleny troughs, where the AABW layer is relatively thin; (4) along the deep flanks of bottom ridges and plateaus like the Mid-Atlantic Ridge, Southwest Indian Ridge, Kerguelen Plateau, Southeast Indian Ridge and Pacific–Antarctic Ridge, where abyssal boundary currents swiftly move AABW away from its multiple sources; and (5) within the axial interior of the Weddell Gyre, where Ekman pumping supplements the density-driven forcing. We note that although all together these locations only occupy 25% of the total area of $\gamma^n = 28.27$ kg m^{-3} (Fig. 16), they account for as much as 45% of the total vertical upwelling of AABW. The highest (turbulent) speeds ($W > 25 \times 10^{-7}$ m s^{-1}) only appear at a few grid points near the South Scotia Ridge, South Sandwich Arc and the Balleny Fracture Zone.

The non-uniform upwelling field depicted in Fig. 15 yields 12.3 Sv as the total volume transport of AABW across the top isopycnal, a figure quite consistent with two previous global estimates of AABW production derived from property budgets over the Antarctic shelves (Carmack, 1977; Jacobs, Fairbanks & Horibe, 1985) and our own CFC-budget. Our oceanic estimate of AABW production makes no assumptions on residence time-scales for the Shelf Water nor of their mixing rates with deeper ambient waters. We compensate for the direct inflow of newly-formed AABW types around the Antarctic continental margins by a highly subjective parametrization of the vertical velocities at the top isopycnal. Despite the fact that the upwelling field shown in Fig. 15 varies over much of the range listed in Table 6, the mean upward speed at $\gamma^n = 28.27$ kg m^{-3} (3.7×10^{-7} m s^{-1}) also compares well with the

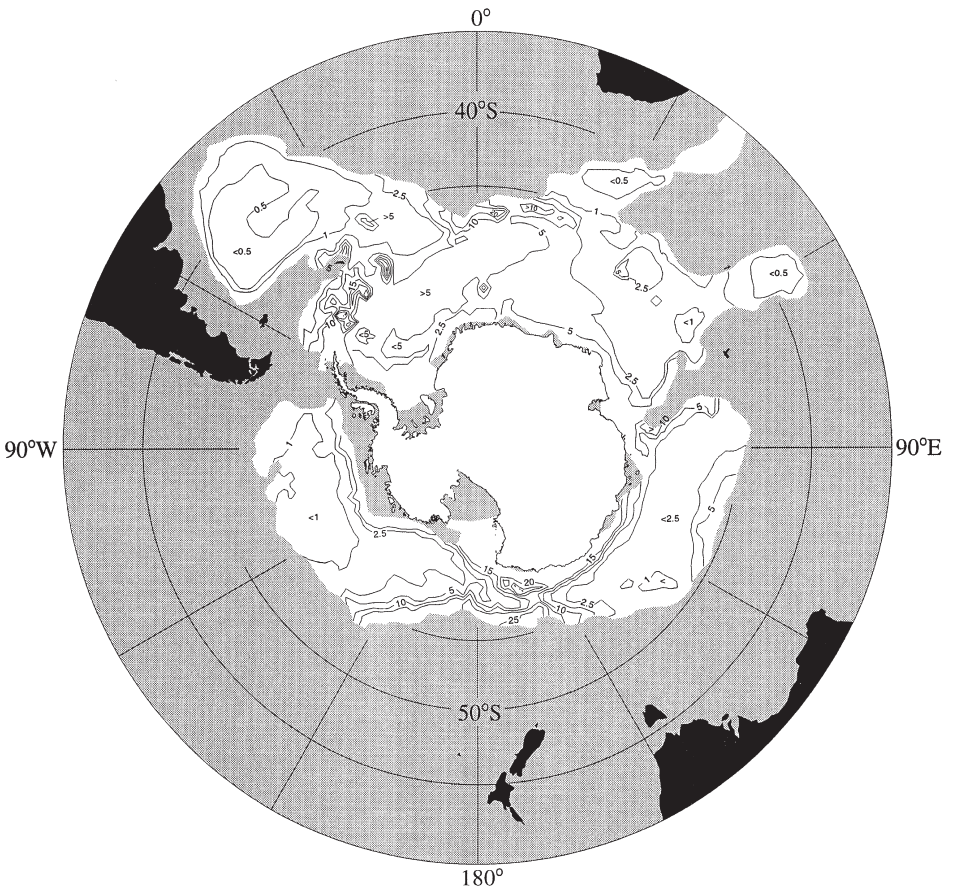

Fig. 15. Global distribution of modeled upwelling speed ($m\ s^{-1}$) at the top of the Antarctic Bottom Water, $\gamma^n = 28.27\ kg\ m^{-3}$.

average of previous estimates of constant deep upwelling rates at 2000 m in all three Ocean Basins to the north. That our ad-hoc distribution of the AABW sinks gives reasonable results is encouraging, but perhaps fortuitous.

To contrast the strengths of all sources in the Atlantic sector against those in the Indian and Pacific sectors combined, if one assumes for a moment that there is no net transport of AABW through the Princess Elizabeth Trough, the model just presented suggests that as much as 7.3 Sv of ABBW (60% of the total) ought to be produced by all the sources along the periphery of the Weddell–Enderby Basin. The remaining 5 Sv of AABW would have to be formed along the shelves of the Adélie-Wilkes Coast and Ross Sea. However, due to the low stability of the thermocline in the interior of the Weddell Gyre, it means that drastic changes in the wind stress and sea-ice conditions, or even sporadic passages of energetic mesoscale features, could easily alter the production rate estimated here for the Atlantic sector. As Gordon

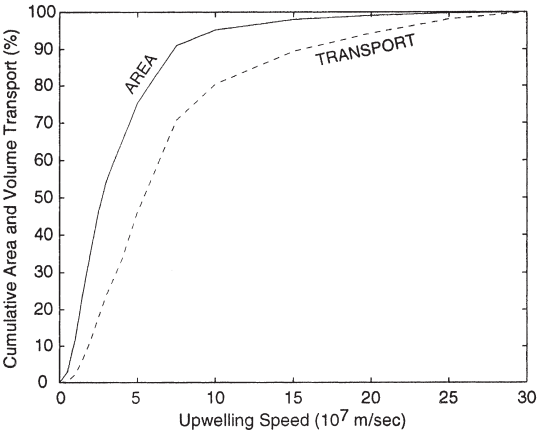

Fig. 16. Relative contributions of the various upwelling regimes shown in Fig. 15 to the estimated total production rate of Antarctic Bottom Water.

(1978, 1982, 1991) and Gordon and Huber (1984, 1990, 1995) point out, a suite of triggering events could switch the whole cyclonic interior region into an unstable mode. This in turn could lead to wide-spread open-ocean convection that, by piercing through $\gamma^n = 28.27$ kg m^{-3}, might contribute unknown volumes of additional AABW to the bottom layer—a mechanism neglected in our estimates.

6. Summary

By exporting bottom waters the Southern Ocean ventilates the vast majority of the deep waters in the rest of the World Ocean. Hence, the strength of the southern source of cold bottom waters and their subsequent equatorward flow are key elements of the Global Thermohaline Circulation. It is clear that deep waters branching off the Antarctic Circumpolar Current supply all of the observed Abyssal Boundary Currents, filling the bottom layers over most of the Southern Hemisphere.

The Drake Passage sill effectively blocks any continuous flow of relatively dense bottom waters between the Antarctic basins of the Pacific and Atlantic Oceans, and so it provides a clear criterion whereby the two distinct components of bottom water with southern origin can be distinguished. One is the voluminous deep water mass carried continuously to the east by the Antarctic Circumpolar Current, namely the Circumpolar Deep Water. The other water mass is too dense to clear the sill of Drake Passage, and so it is not circumpolar in extent. Its ultimate sources are found over the Antarctic margins. Therefore, allowing for mixing along flow paths we define Antarctic Bottom Water as all volumes of water formed to the south of the Antarctic Circumpolar Current with neutral densities greater than 27.28 kg m^{-3}, which are not seen at the Drake Passage sill.

Contributors to the AABW layer are found at several locations around Antarctica,

where Shelf Water with almost freezing temperatures mixes with Circumpolar Deep Water near the shelf break to produce the densest ($\gamma^n > 28.40$ kg m^{-3}) regional types of Antarctic Bottom Water, all of which recirculate within the adjacent oceanic domains. Extreme characteristics of these AABW varieties derive from the local types of Shelf Water. Low-salinity types of AABW are more widely found, in the western Weddell Sea, near the Amery Basin, off the Adélie Land, and in the eastern Ross Sea; whereas a high-salinity type of AABW originates only in the western Ross Sea. Flow of all of these newly formed AABW types away from their sources is westward along the Antarctic slope. This flow is revealed by a remarkable maximum in the average CFC concentrations for $\gamma^n > 28.27$ kg m^{-3}.

Bottom maps of neutral density in the Southern Ocean demonstrate that Antarctic Bottom Water circulates at great depths inside the Australian–Antarctic and Southeast Pacific basins, since it cannot escape the ridge systems surrounding those basins. In contrast, neither the South Scotia Ridge nor the South Sandwich Island Arc can block the northward outflow of AABW from the Weddell Sea, namely Weddell Sea Deep Water, into the Scotia, Georgia and Argentine basins.

On the average, AABW in the Atlantic sector is the coldest and lowest in salinity throughout the Southern Ocean. Volumetric mean temperatures and salinities progressively increase toward the eastern Antarctic Basins. However, the mean CFC concentrations are the highest overall in the Australian–Antarctic Basin, reflecting the combined effects from local sources of AABW plus inflows of Ross Sea Bottom Water from the Pacific sector.

Our oceanic CFC-11 inventory for the AABW layer assumes that abyssal ventilation occurs by input of newly formed AABW types sinking over the continental slope. This estimate yields a lower (upper) limit for the total production rate of AABW of 8 Sv (9.5 Sv), which compares well with previous global mass budgets over the shelf regimes.

Using typical values of deep upwelling speeds derived in the three Oceans farther to the north, a total production rate of 10 Sv of AABW is inferred, which is also in good agreement with previous global estimates for AABW production. An ad-hoc spatial distribution of the upwelling speed at the top of the AABW layer is constructed from three components: wind-induced upwelling proportional to the depth of $\gamma^n = 28.27$ kg m^{-3}, topographically-induced upwelling proportional to the bottom depth, and turbulent upwelling proportional to the layer thickness and bottom depth. Integration of this ad-hoc spatially-varying upwelling field results in a similar production rate of AABW (12 Sv).

Cyclonic flow of young AABW types is clearly indicated by distinct high-CFC tongues in all three Antarctic Basins. Bottom waters formed near the Amery Basin are carried westward along the deep portion of the slope toward the southwestern Weddell Sea. There, an even larger signal reflects the outflow of new Weddell Sea Bottom Water leaving the Filchner Depression and extending northward along the Western Boundary Current. In the Australian–Antarctic Basin new Adélie Land Bottom Water flows westward at great depths, but the high-CFC signal continues clockwise against the Kerguelen Plateau and Southeast Indian Ridge. Input of well-ventilated Ross Sea Bottom Water is also clear near the southeastern corner of that Indian

basin. Another boundary current is indicated against the Balleny Ridge, by a CFC-maximum tongue extending around the outer rim of the western Southeast Pacific Basin.

The general circulation of AABW in the oceanic regime of the Southern Ocean involves three cyclonic cells, linked by eastward flow for its lighter portion through two major choke points located at the Princess Elizabeth (80°E, 65°S) and Balleny (160°E, 65°S) troughs. The largest of these subpolar gyres carries Weddell Sea Deep Water over portions of the Scotia, Georgia and Argentine Basins before returning some of it to the Weddell–Enderby Basin. The progressive ventilation of the ACC by deep and intermediate waters from the Weddell Sea is indicated on vertical sections of CFC across the northern limb of the Weddell Gyre and the southern Argentine Basin.

Enhanced vertical mixing and upwelling at the top of AABW is suggested over the shallow topography of the South Scotia Ridge and southern Scotia Sea. CFC distributions along the top isopycnal of the AABW layer also reflects the existence of locations where rapid upward ventilation and upwelling is enhanced. Even though these areas occupy only a fraction of the total areal coverage of the AABW they probably contribute almost half of the total vertical transport into the lighter waters above.

7. Acknowledgements

Support was provided by the Joint Institute for the Study of the Atmosphere and Ocean (JISAO) under NOAA Cooperative Agreement NA37RJ0198, and by grants to the Pacific Marine Environmental Laboratory (PMEL) from the Climate and Global Change Program through the NOAA Office of Global Programs. This paper is JISAO Contribution Number 474 and PMEL Contribution Number 1869. Construction of the global distributions presented in this work was only possible due to the hard work and generous contributions from many colleagues involved in the WOCE program in the Southern Ocean, among them are Drs Swift, Reid, Talley, Rintoul, McCartney, Nowlin, Whitworth and Fahrbach. Thanks for their permission to use preliminary WOCE data in this study. Much of the CFC discussions and results could not have been done without preliminary measurements made so kindly available by Drs Smethie, Weiss and Warner. We would like thank Arnold L. Gordon for his encouragement to pursue the mass budget for the AABW layer, and Thomas Whitworth III for his constructive comments on an early version of this manuscript.

8. References

Bullister, J. L. (1989). Chlorofluorocarbons as time-dependent tracers in the ocean. *Oceanography*, 12–14.

Carmack, E. C. (1973). Silicate and potential temperature in the deep and bottom waters of the western Weddell Sea. *Deep-Sea Research, 20,* 927–932.

Carmack, E. C. (1977). Water characteristics of the Southern Ocean south of the Polar Front. In M. Angel (Ed.), A Voyage of Discovery, *Deep-Sea Research,* 24(Suppl.).

Carmack, E. C., & Foster, T. D. (1975). On the flow of water out of the Weddell Sea. *Deep-Sea Research, 22*, 711–724.

Coles, V. J., McCartney, M. S., Olson, D. B., & Smethie, W. M. (1996). Changes in Antarctic Bottom Water properties in the western South Atlantic in the late 1980s. *Journal of Geophysical Research, 101*, 8957–8970.

Deacon, G. E. R. (1933). A general account of the hydrology of the South Atlantic Ocean. *Discovery Reports*, 7, 171–238.

Doney, S. C., & Bullister, J. L. (1992). A cholofluorocarbon section in the eastern North Atlantic. *Deep-Sea Research I, 39*, 1857–1883.

Fahrbach, E., Rohardt, G., Scheele, N., Schröeder, M., Strass, V., & Wisotzki, A. (1995). Formation and discharge of deep and bottom water in the northwestern Weddell Sea. *Journal of Marine Research, 53*, 515–538.

Foldvik, A., Gammelsrod, T., & Torresen, T. (1985). Circulation and water masses on the southern Weddell Sea shelf. In S. S. Jacobs, *Oceanology of the Antarctic Continental Shelf* (Vol. 43, pp. 5–20), Antarctic Research Series. Washington, DC: American Geophysical Union.

Foster, T. D., & Carmack, E. C. (1976). Frontal zone mixing and Antarctic Bottom Water formation in the southern Weddell Sea. *Deep-Sea Research, 23*, 301–317.

Gill, A. E. (1973). Circulation and bottom water formation in the Weddell Sea. *Deep-Sea Research, 20*, 111–140.

Gill, A. E. (1977). The hydraulics of rotating channel flow. *Journal of Fluid Mechanics, 80*, 641–671.

Gordon, A. L. (1966). Potential temperature, oxygen and circulation of bottom water in the Southern Ocean. *Deep-Sea Research, 13*, 1125–1138.

Gordon, A. L. (1967). Structure of Antarctic waters between 20°W and 170°W. In V. C. Bushell (Ed.), *Antarctic Map Folio Series* (folio 6). New York: American Geographic Society.

Gordon, A. L. (1971). Oceanography of Antarctic waters. In: J. L. Reid (Ed.), *Antarctic Oceanography I* (Vol. 15, pp. 169–203), Antarctic Research Series. Washington, DC: American Geophysical Union.

Gordon, A. L. (1972). Spreading of Antarctic Bottom Waters, II. In: *Studies in Physical Oceanography—a tribute of George Wüst on his 80th birthday* (Vol. II, pp. 1–17). New York: Gordon and Breach.

Gordon, A. L. (1974). Varieties and variability of Antarctic bottom water. Colloques internationaux du Centre National de la Recherche Scientifique No. 215, Processus de Formation des Eaux Oceaniques Profondes (pp. 33–47).

Gordon, A. L. (1975). An Antarctic oceanographic section along 170°E. *Deep-Sea Research, 22*, 357–377.

Gordon, A. L. (1978). Deep Antarctic convection west of the Maud Rise. *Journal of Physical Oceanography, 8*(4), 600–612.

Gordon, A. L. (1982). Weddell deep water variability. *Journal Marine Research, 40*(Suppl.), 199–217.

Gordon, A. L. (1991). Two stable modes of Southern Ocean winter stratification. In J. Gascard, & P. Chu (Eds.), *Deep convection and water mass formation in the ocean* (pp. 17–35). New York: Elsevier.

Gordon, A. L. (1998). Western Weddell Sea thermohaline stratification. In S. S. Jacobs & R. F. Weiss, *Interactions at the Antarctic continental margins* (Vol. 75, pp. 215–240), Antarctic Research Series. Washington, DC: American Geophysical Union.

Gordon, A. L., & Tchernia, P. T. (1972). Waters of the continental margin off Adélie Coast, Antarctica. In D. E. Hayes (Ed.), *Antarctic Oceanography II: The Australian-New Zealand sector* (Vol. 9, pp. 59–69), Antarctic Research Series. Washington, DC: American Geophysical Union.

Gordon, A. L., & Huber, B. A. (1984). Thermohaline stratification below the Southern Ocean sea ice. *Journal Geophysical Research, 89*(C1), 641–648.

Gordon, A. L., & Huber, B. A. (1990). Southern Ocean winter mixed layer. *Journal Geophysical Research, 95*(C7), 11655–11672.

Gordon, A. L., & Huber, B. A. (1995). Warm Weddell Deep Water west of Maud Rise. *Journal Geophysical Research, 100*(C7), 13747–13753.

Gordon, A. L., Huber, B. A., Hellmer, H., & Ffield, A. (1993). Deep and Bottom Water of the Weddell Sea's western rim. *Science, 262*(5130), 95–97.

Hogg, N. H., Biscaye, P., Gardner, W., & Schmitz, W.J. (1982). On the transport and modification of Antarctic Bottom Water in the Vema Channel. *Journal of Marine Research, 40*(Supp.), 231–263.

IOC, IHO, BODC (1994). Supporting volume to the GEBCO Digital Atlas. British Oceanographic Data Centre.

Jackett, D. R., & MacDougall, T. J. (1997). A neutral density variable for the world's oceans. *Journal of Physical Oceanography*, *27*, 237–263.

Jacobs, S. S. (1965). Physical and chemical oceanographic observations in the Southern Ocean. U.S.N.S. Eltanin cruises 7–15, 1963–64. Technical Report Lamont Geological Observatory, 1–CU–1–65.

Jacobs, S. S., & Georgi, D. T. (1977). Observations on the southwest Indian/Antarctic Ocean. In M. Angel (Ed.), *Voyage of discovery* (pp. 43–85). New York: Pergamon.

Jacobs, S. S., & Haines, W. E. (1982). Oceanographic data in the Ross Sea and along George V Coast, 1976–1979. *Lamont-Doherty Geological Observatory of Columbia University Reference 82-1*. New York: Palisades.

Jacobs, S. S., Amos, A. F., & Bruchhausen, P. M. (1970). Ross Sea oceanography and Antarctic Bottom Water formation. *Deep-Sea Research*, *17*, 935–962.

Jacobs, S. S., Fairbanks, R. G., & Horibe, Y. (1985). Origin and evolution of water masses near the Antarctic Continental Margin: evidence from $H_2{}^{18}O/H_2{}^{16}O$ ratios in seawater. In: *Oceanology of the Antarctic Continental Shelf* (Vol. 43, pp. 59–85), Antarctic Research Series. Washington, DC: American Geophysical Union.

Johnson, G. C. (1990). *Near-equatorial deep circulation in the Indian and Pacific Oceans*. Ph.D. Thesis, MIT/WHOI, WHOI-90-50.

Kunze, E., & Sanford, T. B. (1996). Abyssal mixing: Where it is not? *Journal of Physical Oceanography*, *26*, 2286–2296.

Locarnini, R. A., Whitworth III, T., & Nowlin, W. D. (1993). The importance of the Scotia Sea on the outflow of Weddell Sea Deep Water. *Journal Marine Research*, *51*, 135–153.

Locarnini, R. A. (1994). *Water masses and circulation in the Ross Gyre and environs*. Ph.D. Dissertation, Texas A&M University, College Station.

Lynn, R. J., & Reid, J. L. (1968). Characteristics and circulation of deep and abyssal waters. *Deep-Sea Research*, *15*, 577–598.

Mantyla, A. W., & Reid, J. L. (1983). Abyssal characteristics of the World Ocean waters. *Deep-Sea Research*, *30*, 805–833.

Mantyla, A. W., & Reid, J. L. (1995). On the origins of deep and bottom waters of the Indian Ocean. *Journal Geophysical Research*, *100*(C2), 2417–2439.

Mensch, M., Bayer, R., Bullister, J. L., Schlosser, P., & Weiss, R. F. (1997). The distribution of tritium and CFCs in the Weddell Sea during the mid 1980s. *Progress in Oceanography*, *38*, 377–414.

Muench, R. D., & Gordon, A. L. (1995). Circulation and transport of water along the western Weddell Sea margin. *Journal Geophysical Research*, *100*(C9), 18503–18515.

Munk, W. (1966). Abyssal recipes. *Deep-Sea Research*, *13*, 707–730.

NODC (1994). World Ocean Atlas. U.S. Department of Commerce, National Oceanic and Atmospheric Administration, Washington DC.

Nowlin, W. D., Whitworth III, T., & Pillsbury, R. D. (1977). Structure and transport of the Antarctic Circumpolar Current at Drake Passage from short-term measurements. *Journal of Physical Oceanography*, *7*, 788–802.

Nowlin, W. D., & Zenk, W. (1988). Westward bottom currents along the margin of the South Shetland Island Arc. *Deep-Sea Research*, *35*, 269–301.

Orsi, A. H., & Bullister, J. L. (1996). Synthesis of WOCE Chlorofluorocarbon data in the Pacific Ocean. *U.S. WOCE Report* (pp. 11–13).

Orsi, A. H., Nowlin, W. D., & Whitworth III, T. (1993). On the circulation and stratification of the Weddell Gyre. *Deep-Sea Research I*, *40*, 169–203.

Orsi, A. H., Whitworth III, T., & Nowlin, W. D. (1995). On the meridional extent and fronts of the Antarctic Circumpolar Current. *Deep-Sea Research I*, *42*(5), 641–673.

Patterson, S. L., & Sievers, H. A. (1980). The Weddell–Scotia Confluence. *Journal of Physical Oceanography*, *10*, 1584–1610.

Peterson, R. G., & Whitworth III, T. (1989). The Subantarctic and Polar Fronts in relation to deep water masses through the southwestern Atlantic. *Journal of Geophysical Research*, *94*, 10817–10838.

Polzin, K. L., Speer, K., Toole, J. M., & Schmitt, R. W. (1996). Intense mixing of Antarctic Bottom Water in the equatorial Atlantic. *Nature, London, 380*, 54–57.

Reid, J. L. (1979). On the contribution of the Mediterranean Sea outflow to the Norwegian-Greenland Sea. *Deep-Sea Research, 26*, 1199–1223.

Reid, J. L. (1990). On the total geostrophic circulation of the South Atlantic Ocean: Flow patterns, tracers, and transports. *Progress in Oceanography, 23*, 149–244.

Reid, J. L., Nowlin, W. D., & Patzert, W. C. (1977). On the characteristics and circulation of the southwestern Atlantic Ocean. *Journal of Physical Oceanography, 7*, 62–91.

Reid, J. L., & Lynn, R. J. (1971). On the influence of the Norwegian-Greenland and Weddell seas upon the bottom waters of the Indian and Pacific oceans. *Deep-Sea Research, 18*, 1063–1088.

Rintoul, S. R., & Bullister, J. L. (1999). A late winter hydrographic section from Tasmania to Antarctica. *Deep-Sea Research* I, 46, 1417–1454.

Rintoul, S. R. (1998). On the origin and influence of Adélie Land Bottom Water. In S. S. Jacobs & R. F. Weiss (Eds.), *Interactions at the Antarctic Continental Margins*, (Vol. 75, pp 151–171) Antarctic Research Series. Washington, DC: American Geophysical Union.

Robbins, P. E., & Toole, J. M. (1997). The dissolved silica budget as a constraint on the meridional overturning circulation of the Indian Ocean. *Deep-Sea Research I* 44, 879–906.

Robbins, P. E., & Bryden, H. L. (1994). Direct observations of advective nutrient and oxygen fluxes at 24°N in the Pacific Ocean. *Deep-Sea Research I, 41*, 143–168.

Rodman, M. R., & Gordon, A. L. (1982). Southern Ocean Bottom Water of the Australian–New Zealand Sector. *Journal Geophysical Research, 87*, 5771–5778.

Roether, W., Schlitzer, R., Putzka, A., Beining, P., Bulsiewicz, K., Rohardt, G., & Delahoyde, F. (1993). A chlorofluoromethane and hydrographic section across Drake Passage: Deep water ventilation and meridional property transport. *Journal of Geophysical Research, 98*, 14423–14435.

Roemmich, D. (1983). Optimal estimation of hydrographic station data and derived fields. *Journal of Physical Oceanography, 13*, 1544–1549.

Roemmich, D., Hautala, S., & Rudnick, D. (1996). Northward abyssal transport through the Samoan passage and adjacent regions. *Journal of Geophysical Research, 101*(C6), 14039–14055.

Schlemmer, F. C. (1978). *Structure and spreading of antarctic waters in the ocean basins adjacent to Antarctica*. Ph.D. Dissertation, Texas A&M University, College Station.

Schlosser, P., Bullister, J. L., & Bayer, R. (1991). Studies of dep water formation and circulation in the Weddell Sea using natural and anthropogenic tracers. *Marine Chemistry, 35*, 97–122.

Schmitz, W. J. (1995). On the interbasin-scale thermohaline circulation. *Reviews of Geophysics, 33*, 151–173.

Scripps Institution of Oceanography/Texas A&M University (1985). Physical, chemical and in situ CTD data from the Ajax expedition in the South Atlantic Ocean. *SIO Reference 85–24, TAMU Reference 84-4*. La Jolla, CA: Scripps Institution of Oceanography.

Schnack-Schiel, S. (1987). The winter-expedition of RV Polarstern to the Antarctic (ANT V/1-3). In *Berichte zur Polarforschung* (Vol. 39). Bremerhaven: Alfred-Wegener-Institute.

Sievers, H. A., & Nowlin, W. D. (1984). The stratification and water masses at Drake Passage. *Journal Geophysical Research, 89*(C6), 10489–10514.

Speer, K. G., & Forbes, A. (1994). A deep western boundary current in the South Indian Basin. *Deep-Sea Research I, 41*(9), 1289–1303.

Speer, K. G., & Zenk, W. (1993). The flow of Antarctic Bottom Water into the Brazil Basin. *Journal of Physical Oceanography, 23*, 2667–2682.

Stommel, H. (1958). The abyssal circulation. *Deep-Sea Research, 5*, 80–82.

Stommel, H., & Arons, A. B. (1960). On the abyssal circulation of the world ocean—I. Stationary planetary flow patterns on a sphere. *Deep-Sea Research, 6*, 140–154.

Stommel, H., & Arons, A. B. (1960). On the abyssal circulation of the world ocean—II. An idealized model of the circulation pattern and amplitude in oceanic basins. *Deep-Sea Research, 6*, 217–233.

Sverdrup, H. U. (1940). Hydrology, Section 2, discussion. Report B.A.N.Z. *Antarctic Research Expedition 1921–31* (Series A, Vol. 3, pp. 88–126). Oceanography, Part 2, Section 2.

Tchernia, P., & Jeannin, P. F. (1983). Quelques aspects de la circulation océanique Antarctique réveles

par l'observation de la dérive d'icebergs (1972–1983). Céntre National d'Etudes Spatiales. Paris: Mus. Nat. Hist. Nat..

Toole, J. M., & Warren, B. A. (1993). A hydrographic section across the subtropical South Indian Ocean. *Deep-Sea Research I, 40*, 1973–2019.

Toole, J. M., Polzin, K. L., & Schmitt, R. W. (1994). Estimates of diapycnal mixing in the abyssal ocean. *Science, 264*, 1120–1123.

Trumbore, S. E., Jacobs, S. S., & Smethie, W. M. (1991). Chlorofluorocarbon evidence for rapid ventilation of the Ross Sea. *Deep-Sea Research, 38*, 845–870.

Tsuchiya, M., Talley, L. D., & McCartney, M. S. (1994). Water-mass distributions in the western South Atlantic; A section from South Georgia Island (54°S) northward across the equator. *Journal of Marine Research, 52*, 55–81.

Van Scoy, K. A., Locarnini, R. A., Watson, A. J., Meredith, M. P., Heywood, K. J. & King, B. A. (1999). On the sources of Weddell Gyre Antarctic Bottom Water, *Journal of Geophysical Research*, in press.

Warner, M. J., & Weiss, R. F. (1988). Solubilities of chlorofluorocarbons 11 and 12 in water and seawater. *Deep-Sea Research, 32*, 1485–1497.

Warner, M. J., & Weiss, R. F. (1992). Chlorofluoromethanes in South Atlantic Antarctic Intermediate Water. *Deep-Sea Research, 39*, 2053–2075.

Warren, B. A. (1981). Transindian hydrographic section at Lat. 18°S: Property distributions and circulation in the South Indian Ocean. *Deep-Sea Research, 28*, 759–788.

Warren, B. A. (1981). Transindian hydrographic section at Lat. 18°S: Property distributions and circulation in the South Indian Ocean. *Deep-Sea Research, 28A*(8), 759–788.

Warren, B. A., & Speer, K. G. (1991). Deep circulation in the eastern South Atlantic Ocean. *Deep-Sea Research, 38*(Suppl.1), S281–S322.

Weiss, R. F. (1987). Winter Weddell Sea Project 1986: Trace gas studies during legs ANT V/2 and V/3 of Polarstern. *Antarctic Journal of the U.S., 22*(5), 99–100.

Weiss, R. F., Östlund, G., & Craig, H. (1979). Geochemical studies of the Weddell Sea. *Deep-Sea Research, 26*, 1093–1120.

Weiss, R. F., Bullister, J. L., Warner, M. J., Van Woy, F. A., & Salameh, P. K. (1990). Ajax expedition chlorofluorocarbon measurements. Scripps Institution of Oceanography, Reference 90-6.

Weiss, R. F., Warner, M. J., Salameh, P. K., Van Woy, F. A., & Harrison, K. G. (1993). South Atlantic Ventilation Experiment: SIO Chlorofluorocerbon Measurements. Scripps Institution of Oceanography, Reference 93-49.

Weppernig, R., Schlosser, P., Khatiwala, S., & Fairbanks, R. G. (1996). Isotope data from Ice Station Weddell: Implications for deep water formation in the western Weddell Sea. *Journal of Geophysical Research, 101*, 25723–25739.

Whitehead, J. A., & Worthington, L. V. (1982). The flux and mixing rates of Antarctic Bottom Water within the North Atlantic. *Journal of Geophysical Research, 87*, 7903–7924.

Whitworth III, T., & Nowlin, W. D. (1987). Water masses and currents of the southern ocean at the Greenwhich Meridian. *Journal of Geophysical Research, 92*, 6462–6476.

Whitworth III, T., Nowlin, W. D., & Worley, S. J. (1982). The net transport of the Antarctic Circumpolar Current through Drake Passage. *Journal of Physical Oceanography, 12*, 960–971.

Whitworth III, T., Nowlin, W. D., Orsi, A. H., Locarnini, R. A., & Smith, S. G. (1994). Weddell Sea Shelf Water in the Bransfield Strait and Weddell–Scotia Confluence. *Deep-Sea Research I, 41*, 629–641.

Whitworth III, T., Nowlin, W. D., Pillsbury, R. D., Moore, M. I., & Weiss, R. F. (1991). Observations of the Antarctic Circumpolar Current and deep western boundary current in the southwestern Atlantic. *Journal of Geophysical Research, 96*, 15105–15118.

Whitworth III, T., Orsi, A. H., Kim, S. J., Nowlin Jr., W. D., & Locarnini, R. A. (1998). Water masses and mixing near the Antarctic Slope Front. In S. S. Jacobs & R. F. Weiss (Eds.), *Interactions at the Antarctic Continental Margins* (Vol. 74, pp. 1–27), Antarctic Research Series. Washington, DC: American Geophysical Union.

Wüst, G. (1933). Das Bodenwasser und die Gliederung der Atlantischen Tiefsee. *Wiss. Ergebn. Dtsh. Atlant. Exped. auf dem Forschungs- und Vermessungsschiff 'Meteor', 6*(1)(1), 1–107.

Wüst, G. (1935). Schichtung und Zirkulation des Atlantischen Ozeans. Die Stratosphäre. *Wissenschaftliche*

Ergebnisse der Deutschen Atlantischen Expedition auf dem Forschungs- und Vermessungsschiff 'Meteor' 11925–1927, *6*(1st Part, 2).